Non-parametric Data Assimilation Scheme for Land Hydrological Applications

M. Khaki[a,1], F. Hamilton[b], E. Forootan[c], I. Hoteit[d], J. Awange[a], M. Kuhn[a]

[a]*School of Earth and Planetary Sciences, Discipline of Spatial Sciences, Curtin University, Perth, Australia.*
[b]*North Carolina State University, Raleigh, North Carolina 27695, USA.*
[c]*School of Earth and Ocean Sciences, Cardiff University, Cardiff, UK.*
[d]*King Abdullah University of Science and Technology, Thuwal, Saudi Arabia.*

Abstract

Data assimilation, which relies on explicit knowledge of dynamical models, is a well-known approach that addresses models' limitations due to various reasons, such as errors in input and forcing datasets. This approach, however, requires intensive computational efforts, especially for high dimensional systems such as distributed hydrological models. Alternatively, data-driven methods offer comparable solutions when the physics underlying the models are unknown. For the first time in a hydrological context, a non-parametric framework is implemented here to improve model estimates using available observations. This method uses Takens delay-coordinate method to reconstruct the dynamics of the system within a Kalman filtering framework, called the Kalman-Takens filter. A synthetic experiment is undertaken to fully investigate the capability of the proposed method by comparing its performance with that of a standard assimilation framework based on an adaptive unscented Kalman filter (AUKF). Furthermore, using terrestrial water storage (TWS) estimates obtained from the Gravity Recovery And Climate Experiment (GRACE) mission, both filters are applied to a real case scenario to update different water storages over Australia. In-situ groundwater and soil moisture measurements within Australia are used to further evaluate the results. The Kalman-Takens filter successfully improves the estimated water storages at levels comparable to the AUKF results, with an average RMSE reduction of 37.30% for groundwater and 12.11% for soil moisture estimates. Additionally, the Kalman-Takens filter, while reducing estimation complexities, requires a fraction of the computational time, i.e., ∼8 times faster compared to the AUKF approach.

Keywords: Non-parametric filtering, Data assimilation, Data-driven, Kalman-Takens, Adaptive unscented Kalman filtering (AUKF), Hydrological modelling.

Email address: Mehdi.Khaki@postgrad.curtin.edu.au (M. Khaki)

1. Introduction

A precise study of terrestrial water storage (TWS) changes is essential to better understand the spatio-temporal variations of water resources and their effects on the hydrological cycles. In this regard, hydrological models become valuable tools for simulating hydrological processes at global (e.g., Döll et al., 2003; Huntington, 2006; Coumou and Rahmstorf, 2012; van Dijk et al., 2013) and regional (e.g., Chiew et al., 1993; Wooldridge and Kalma, 2001; Christiansen et al., 2007; Huang et al., 2016) scales. These models are formulated based on physical/conceptual principles to represent 'reality' and are still being developed to accurately simulate all complex hydrological processes, including interactions between water cycle components (e.g., surface and sub-surface water exchange). These models, however, can be subject to various sources of uncertainties, e.g., errors in input and forcing data, and imperfect accounting for the physical underlying dynamics, such as those used to simulate evapotranspiration (van Dijk et al., 2011; Vrugt et al., 2013).

Classically, data assimilation can be used to improve imperfect models by integrating available observations with the underlying physical model. Many studies have implemented data assimilation techniques in the fields of ocean and atmospheric sciences (e.g., Bennett, 2002; Hoteit et al., 2002; Kalnay, 2003; Schunk et al., 2004; Lahoz, 2007; Zhang et al., 2012; Hoteit et al., 2012; Tardif et al., 2015; Zhao et al., 2017) and hydrology (e.g., Seo et al., 2003; Vrugt et al., 2005; Weerts and El Serafy, 2006; Rasmussen et al., 2015; Kumar et al., 2016; Girotto et al., 2016, 2017; Schumacher et al., 2018). Data assimilation is often used to improve model simulations of soil moisture (e.g., Entekhabi et al., 1994; Calvet et al., 1998; Montaldo et al., 2001; Reichle et al., 2002; De Lannoy et al., 2007, 2009; Kumar et al., 2009; Brocca et al., 2010; Renzullo et al., 2014; Kumar et al., 2015; Lievens et al., 2015; De Lannoy et al., 2015), TWS (e.g., Zaitchik et al., 2008; van Dijk et al., 2014; Tangdamrongsub et al., 2015; Schumacher et al., 2016, 2018; Khaki et al., 2017a, 2018a,b), evapotranspiration and sensible heat fluxes (e.g., Schuurmans et al., 2003; Pipunic et al., 2008; Irmak and Kamble, 2009; Yin et al., 2014), surface water and river discharge (e.g., Bras and Restrepo-Posada, 1980; Awwad et al., 1994; Young, 2002; Madsen and Skotner, 2005; Vrugt et al., 2006; Andreadis et al., 2007; Neal et al., 2009; Giustarini et al., 2011; Lee et al., 2011; McMillan et al., 2013; Li et al., 2015). Standard data assimilation techniques have their limitations though, e.g., the general requirement of intensive computations for high dimensional systems in realistic applications (Tandeo et al., 2015). Furthermore, when a physical model (i.e., model's underlying equations) is not available,

the application of a traditional data assimilation framework that relies on these equations for forecasting can be limited (see, e.g., Palmer, 2001; Reichle and Koster, 2005; Hersbach et al., 2007; Arnold et al., 2013).

A number of studies employ data-driven (non-parametric) approaches to produce accurate statistical simulations (e.g., Sauer, 2004; Tandeo et al., 2015; Dreano et al., 2015; Hamilton et al., 2016; Lguensat et al., 2017). Hamilton et al. (2015) and Berry and Harlim (2016) considered the case when models are partially known. In other cases with completely unknown systems, e.g., no available information about the physics of the underlying models and correspondingly their equations, the application of data assimilation becomes rather complicated. Hamilton et al. (2016) developed a new model-free filter based on the non-parametric Takens approach and Kalman filtering when the physical model is not available. The main idea of Takens' theorem is that the model equations can be replaced by a data-driven non-parametric reconstruction of the system's dynamics. The filter implements Takens' method for attractor reconstruction within the Kalman filtering framework, allowing for a model-free approach to filter noisy data (Hamilton et al., 2016). Takens method has been used in various studies for non-parametric time series predictions (see, e.g., Packard et al., 1980; Takens, 1981; Sauer et al., 1991; Sauer, 2004). This technique replaced the model with a delay coordinate embedding scheme and has been shown by Hamilton et al. (2016) to not only obtain comparable results to a standard Kalman filter-based framework, but also may perform better when model errors are significant. A similar idea has been used by Tandeo et al. (2015) and Lguensat et al. (2017) to simulate the dynamics of complex systems using a non-parametric sampler. They applied an Analog Data Assimilation (AnDA) scheme that reconstructs the system's dynamics in a fully data-driven manner. While AnDA does not require knowledge of the dynamical model, it assumes that a representative catalog of trajectories of the system is available. They show that the data-driven method performs well without using the physical model.

The main motivation of this study, therefore, is to apply for the first time the Kalman-Takens method in a hydrological context and investigate its capability to enhance a hydrological model's estimates. Its performance is then compared with that of a traditional data assimilation system. The motivation behind selecting the Kalman-Takens method is that it does not use the model's equations, and requires less computational burden to predict high-dimensional systems compared to other existing methods (e.g., Hamilton et al., 2015; Tandeo et al., 2015; Berry and Harlim, 2016). This study extends the Kalman-Takens approach to enable its application to

a more complicated state observation transition systems, e.g., for a case of updating various variables (e.g., soil moisture and groundwater) using only TWS observations. The proposed scheme exploits model trajectories for these variables as the training data and is then applied to assimilate TWS data derived from the Gravity Recovery And Climate Experiment (GRACE) satellite mission into the hydrological system states over Australia for the period 2003–2013. It should be pointed out here that the use of model trajectory in this method, and the reliance of data-driven on data in general, results in updating observable state variables only. This, however, is different in a standard data assimilation, which can further update other variables subject to availability of the physical model.

GRACE TWS data have been assimilated in many studies, where they have proved to be highly capable of improving the performance of hydrological models (e.g., Zaitchik et al., 2008; van Dijk et al., 2014; Eicker et al., 2014; Reager et al., 2015; Schumacher et al., 2018). Nevertheless, GRACE data assimilation has always been challenging due to the unique characteristics of its measurements, such as the coarser spatio-temporal resolution compared to most of the existing hydrological models (Khaki et al., 2017b). A successful data assimilation method should be able to account for these limitations in GRACE products while vertically spreading their information into various water compartments (see, e.g., Schumacher et al., 2016; Khaki et al., 2017b). Khaki et al. (2017a) showed that assimilating GRACE data can significantly improve the hydrological model performance over Australia (see also Khaki et al., 2017c; Tian et al., 2017). In order to benchmark the performance of the proposed data-driven technique, its outputs are compared to those of a standard data assimilation framework based on an adaptive unscented Kalman filter (AUKF, Berry et al., 2013). The results of both methods are evaluated against in-situ measurements, as well as through a synthetic experiment to fully investigate their efficiency in assimilating GRACE TWS data.

The remainder of this contribution is organized as follow: datasets are presented in Section 2, the filtering scheme described in Section 3 and the results discussed in Section 4 before concluding the study in Section 5.

2. Model and Data

2.1. W3RA

The 1°×1° version of the World-Wide Water Resources Assessment (W3RA; http://www.wenfo.org/wald/data-software/) model from the Commonwealth Scientific and In-

dustrial Research Organisation (CSIRO) is chosen for the study. The model is designed to simulate landscape water stores and describe the water balance of the soil, groundwater and surface water stores in which each cell is modeled independently of its neighbors (van Dijk, 2010; Renzullo et al., 2014). The model's forcing includes daily meteorological fields of minimum and maximum temperature, short-wave radiation, and precipitation from Princeton University (Sheffield et al., 2006). The model state vector in our experiment is composed of storages of the top, shallow root and deep root soil layers, groundwater, and surface water for the period of January 2003 to December 2012.

2.2. GRACE TWS

For the same period, GRACE level 2 (L2) Stokes' coefficients (up to degree and order 90) and associated full error information are obtained from the ITSG-Grace2014 gravity field model (Mayer-Gürr et al., 2014). Three degree 1 coefficients (C10, C11, and S11) and degree 2 and order 0 (C20) coefficient are replaced by those of Swenson et al. (2008) and that of Cheng and Tapley (2004), respectively. Further, we apply the DDK2 smoothing filter (Kusche et al., 2009) to mitigate a colored/correlated noise in the coefficients (see also Khaki et al., 2018c), and thereafter convert them into $1^\circ \times 1^\circ$ TWS fields following Wahr et al. (1998). The mean TWS for the study period is taken from the W3RA model and is aggregated to the GRACE TWS change time series to reach absolute values related to W3RA (Zaitchik et al., 2008). Error information of ITSG-Grace2014 is used to construct an observation error covariance matrix (Eicker et al., 2014; Schumacher et al., 2016).

2.3. In-situ measurements

In-situ groundwater and soil moisture measurements are used to evaluate the performance of the proposed data assimilation framework. Groundwater data is provided from the New South Wales Government (NSW) within the Murray-Darling Basin, which includes 70% of Australia's irrigated area, covers an area of over one million square kilometers, and extends over much of the central and south-eastern parts of Australia (Mercer et al., 2007). The data is rescaled to a monthly temporal scale to be consistent with GRACE and time series of groundwater storage anomalies. Considering that a specific yield for converting well-water levels to variations in groundwater storage (Rodell et al., 2007; Zaitchik et al., 2008) is not available, we use the value of 0.13 specific yield obtained from the range between 0.115 and 0.2 as suggested by the Australian Bureau of Meteorology (BOM) and Seoane et al. (2013).

Furthermore, in-situ soil moisture products are acquired from the moisture-monitoring network, known as the OzNet network (http://www.oznet.org.au/), over the Murrumbidgee catchment (Smith et al., 2011) and rescaled to the same temporal scale as above. The data contains long-term records of measured volumetric soil moisture at various soil depths at 57 locations across the Murrumbidgee catchment area. Soil measurements at 0–8 cm, the 0–30 cm, and 0–90 cm layers are used to assess the estimated soil moisture results of the proposed assimilation framework. The results can be evaluated using representative soil moisture sites within the basin. Here, we use an analysis suggested by De Lannoy et al. (2007) to acquire the representative soil moisture in-situ measurements (see other methods, in e.g., Famiglietti et al., 2008; Orlowsky and Seneviratne, 2014; Nicolai-Shaw et al., 2015). The method is based on relative differences $d_{m,n}$ for site m and time step n, which can be calculated as (De Lannoy et al., 2007),

$$d_{m,n} = \frac{SM_{m,n} - \overline{SM}_n}{\overline{SM}_n}, \tag{1}$$

where $SM_{m,n}$ is the soil moisture measurement at m and n, and $\overline{SM}_n$ represents the spatially averaged soil moisture. Once $d_{m,n}$ is calculated for each site, the temporally average difference ($\bar{d}_m$) and its standard deviation ($STD(d_m)$) are computed. The most representative site is then the one with $\bar{d}_m$ and $STD(d_m)$ closer to 0.

3. Methodology

3.1. Adaptive Unscented Kalman Filter (AUKF)

Consider the following nonlinear system,

$$\mathbf{x}_t = \mathbf{f}(\mathbf{x_{t-1}}) + \mathbf{v_{t-1}}, \tag{2}$$

$$\mathbf{y}_t = \mathbf{h}(\mathbf{x_t}) + \mathbf{u_t}, \tag{3}$$

where $\mathbf{f}$, the system dynamics, describes the evolution of state vector, $\mathbf{x}$, over time (t) and $\mathbf{h}$, the observation function, maps $\mathbf{x_t}$ to the observations, $\mathbf{y_t}$. $\mathbf{v}_{t-1}$ represent the process noise, which is assumed to be Gaussian with mean 0 and covariance $\mathbf{Q}$. $\mathbf{u}_t$ indicates observation noise with covariance $\mathbf{R}$, which is assumed to be known (see Section 2). In the present study, $\mathbf{x}$ consists of different water storages including top, shallow and deep soil water, vegetation, snow, surface, and groundwater storages while $\mathbf{y}$ represents the GRACE TWS data.

For nonlinear systems, the unscented Kalman filter (UKF) (Julier and Uhlmann, 1997; Julier et al., 2000; Julier and Uhlmann, 2004; Simon, 2006; Wan and van der Merwe, 2001; Terejanu, 2009) can be used for state estimation. The UKF approximates the propagation of the mean and covariance of a random variable through a nonlinear function using a deterministic sampling approach that generates an ensemble of state values known as sigma points. Given the current state and covariance estimates $\mathbf{x}^a_{t-1}$ and $\mathbf{P}^a_{t-1}$ at step t of the filter, $2L+1$ sigma points (where L is the dimension of the state vector) are generated by,

$$\mathbf{x}^0_{t-1} = \mathbf{x}^a_{t-1}, \tag{4}$$

$$\mathbf{x}^i_{t-1} = \mathbf{x}^a_{t-1} + \left(\sqrt{(L+\lambda)\mathbf{P}^a_{t-1}}\right)_i \quad i = 1, \ldots, L, \tag{5}$$

$$\mathbf{x}^{i+L}_{t-1} = \mathbf{x}^a_{t-1} - \left(\sqrt{(L+\lambda)\mathbf{P}^a_{t-1}}\right)_i \quad i = 1, \ldots, L, \tag{6}$$

with $\left(\sqrt{(L+\lambda)\mathbf{P}^a_{t-1}}\right)_i$ being the i^{th} column of the matrix square root (e.g., lower triangular Cholesky factorization, Wan and van der Merwe, 2000) of $(L+\lambda)\mathbf{P}^a_{t-1}$. The corresponding weights to the above sigma points defined as,

$$w^0_s = \frac{\lambda}{(L+\lambda)}, \tag{7}$$

$$w^0_c = \frac{\lambda}{(L+\lambda)} + (1 - \alpha^2 + \beta), \tag{8}$$

$$w^i_s = w^i_c = \frac{1}{2(L+\lambda)} \quad i = 1, \ldots, 2L, \tag{9}$$

where $\sum_{i=0}^{2L} w^i_s = \sum_{i=0}^{2L} w^i_c = 1$. In Eqs. 5–9, λ is the scaling parameter, which can be calculated as $\lambda = \alpha^2(L+\kappa) - L$. The scaling factor α determines the spread of the sigma points around $\mathbf{x}^a_{t-1}$, and κ is a secondary scaling parameter usually set to 0 (the specific value of kappa is not critical, see e.g., Julier and Uhlmann, 1997; Van der Merwe, 2004). β is employed to incorporate a prior knowledge about the noise distribution (e.g., the optimal choice for Gaussian distribution is $\beta = 2$, e.g., Wan and van der Merwe, 2001).

Between these factors, the selection of α has larger impacts on the ensemble spreads and controls the "size" of the sigma-point distribution. α determines how the sigma points can be scaled towards or away from the mean of the prior distribution. For example, $\alpha = 1$ and correspondingly $\lambda = 0$ leads the distance between $\mathbf{x}^a_{t-1}$ and the sigma points to be proportional to $\sqrt{L}$. Positive values of λ (for $\alpha > 1$) scales the sigma points further from $\mathbf{x}^a_{t-1}$ while negative

values of λ (for $\alpha < 1$) scales the sigma points towards $\mathbf{x}^a_{t-1}$. In other words, the larger values for this scaling factor causes a larger spread in the sigma points while smaller values result in more concentration around prior distribution (Van der Merwe, 2004). Ideally α should be a small number, e.g., $1e-4 \leq \alpha \leq 1$ (Song and He, 2005) to avoid sampling non-local effects when the nonlinearities are strong. However, optimal sets of this factor along with κ and β are generally problem specific and can be optimized arbitrary. For the current study, the values of parameters are assumed as $\alpha = 0.5$, $\kappa = 0$, and $\beta = 2$. Nevertheless, it is found that the implemented AUKF is not very sensitive to the parameter selection as long as they result in a numerically well-behaved set of sigma-points and weights (see also Van der Merwe, 2004).

The sigma points are advanced forward one time step using model $\mathbf{f}$ and observed using the function $\mathbf{h}$,

$$\mathbf{x}^{f,j}_t = \mathbf{f}(\mathbf{x}^{\mathbf{j}}_{\mathbf{t-1}}), \quad \mathbf{j} = \mathbf{0}, \ldots, \mathbf{2L}, \tag{10}$$

$$\mathbf{y}^{f,j}_t = \mathbf{h}(\mathbf{x}^{\mathbf{f,j}}_{\mathbf{t}}), \quad \mathbf{j} = \mathbf{0}, \ldots, \mathbf{2L}. \tag{11}$$

The transformed points ($\mathbf{x}^{f,j}_t$ and $\mathbf{y}^{f,j}_t$) are then used to calculate their respective forecast means and covariance matrices,

$$\mathbf{x}^f_t = \sum_{j=0}^{2L} w^j_s \mathbf{x}^{f,j}_t, \tag{12}$$

$$\mathbf{y}^f_t = \sum_{j=0}^{2L} w^j_s \mathbf{y}^{f,j}_t, \tag{13}$$

$$\mathbf{P}^f_t = \sum_{j=0}^{2L} w^j_c \left(\mathbf{x}^{f,j}_t - \mathbf{x}^f_t\right)\left(\mathbf{x}^{f,j}_t - \mathbf{x}^f_t\right)^T + \mathbf{Q}_{t-1}, \tag{14}$$

$$\mathbf{P}_{\mathbf{y}^f_t} = \sum_{j=0}^{2L} w^j_c \left(\mathbf{y}^{f,j}_t - \mathbf{y}^f_t\right)\left(\mathbf{y}^{f,j}_t - \mathbf{y}^f_t\right)^T + \mathbf{R}_t, \tag{15}$$

as well as the cross covariance between $\mathbf{x}^f_t$ and $\mathbf{y}^f_t$,

$$\mathbf{P}_{\mathbf{x}^f_t,\mathbf{y}^f_t} = \sum_{j=0}^{2L} w^j_c \left(\mathbf{x}^{f,j}_t - \mathbf{x}^f_t\right)\left(\mathbf{y}^{f,j}_t - \mathbf{y}^f_t\right)^T. \tag{16}$$

In the analysis step of the filter, the measurements (e.g., GRACE-derived TWS) are used to correct the forecasted state and respective covariance matrix using the Kalman update

equations,

$$\mathbf{x}_t^a = \mathbf{x}_t^f + \mathbf{K}(\mathbf{y}_t - \mathbf{y}_t^f), \tag{17}$$

$$\mathbf{K} = \mathbf{P}_{\mathbf{x}_t^f, \mathbf{y}_t^f} \mathbf{P}^{-1}_{\mathbf{y}_t^f}, \tag{18}$$

$$\mathbf{P}_t^a = \mathbf{P}_{\mathbf{x}_t^f} - \mathbf{K}\mathbf{P}_{\mathbf{y}_t^f}\mathbf{K}^T. \tag{19}$$

where $\mathbf{K}$ is the Kalman gain.

Critical to the success of the UKF is the selection of the filter noise covariances, and in particular the process noise covariance matrix $\mathbf{Q}$. Here, we use the method of Berry et al. (2013) to adaptively estimate this covariance matrix. We refer to this as the *adaptive unscented Kalman filter* (AUKF). Building on the method of Mehra (1990, 1992), the general idea of Berry et al. (2013) is to use the increment, $\epsilon_t = \mathbf{y}_t - \mathbf{y}_t^f$, to estimate the noise covariance at each time step. The method begins by forming an empirical estimate $\mathbf{Q}_{t-1}^e$ for $\mathbf{Q}$,

$$\mathbf{P}_{t-1}^e = \mathbf{F}_{t-1}^{-1}\mathbf{H}_{t-1}^{-1}\epsilon_{t-1}\epsilon_{t-1}^T\mathbf{H}_{t-1}^{-T} + \mathbf{K}_{t-1}\epsilon_{t-1}\epsilon_{t-1}^T\mathbf{H}_{t-1}^{-T}, \tag{20}$$

$$\mathbf{Q}_{t-1}^e = \mathbf{P}_{t-1}^e - \mathbf{F}_{t-2}\mathbf{P}_{t-2}^a\mathbf{F}_{t-2}^T, \tag{21}$$

where $\mathbf{P}_{t-1}^e$ is an empirical estimate of the background covariance. In Eqs. 20 and 21, $\mathbf{F}$ and $\mathbf{H}$ are local linearizations of the nonlinear dynamic models $\mathbf{f}$ and $\mathbf{h}$, respectively, and are estimated using a linear regression on the ensembles (see Eq. 7 in Berry et al., 2013, for details regarding this linearization). It is worth mentioning that we must store linearizations $\mathbf{F}_{t-2}, \mathbf{F}_{t-1}, \mathbf{H}_{t-1}, \mathbf{H}_t$, increments $\epsilon_{t-1}, \epsilon_t$, analysis covariance $\mathbf{P}_{t-2}^a$, and Kalman gain $\mathbf{K}_{t-1}$ from the $t-1$ and $t-2$ steps of the filter. To form a stable estimate of $\mathbf{Q}$, the noisy estimate $\mathbf{Q}_{t-1}^e$ is combined using an exponentially weighted moving average,

$$\mathbf{Q}_t = \mathbf{Q}_{t-1} + (\mathbf{Q}_{t-1}^e - \mathbf{Q}_{t-1})/\tau, \tag{22}$$

where τ is the window of the moving average. Berry et al. (2013); Hamilton et al. (2016) provide additional details on the estimation of noise covariance.

3.2. Kalman-Takens Method

The main idea of the Kalman-Takens method is to replace the model-based forecast in the AUKF with the advancement of the dynamics non-parametrically, thus requiring no knowledge

of $\mathbf{f}$ (in Eq. 2). We provide a brief description of the method below, specifically highlighting modifications in adopting the algorithm to our problem. Full details of the methodology can be found in Hamilton et al. (2016, 2017).

In the present study, we consider a different setup to implement the Kalman-Takens filter for a more complicated state observation transition systems. While the data available are gridded GRACE TWS, our interest is in estimating the different water variables (i.e., top, shallow and deep soil water, vegetation, snow, surface, and groundwater). These variables with no independent observation available, are provided by the W3RA model and are used to produce delay-coordinate vectors. We generate a synthetic set of model trajectories (open-loop run) for these variables to serve as the training data for the Kalman-Takens filter. The training data represents the state of the system. It is also used to generate a local proxy $\tilde{\mathbf{f}}$ for the unknown model $\mathbf{f}$ (cf. Eq. 2), which is not available in the non-parametric framework, so Eq. 10 for advancing the ensemble forward in time in AUKF is not implementable. This brings us to Eq. 23, which defines the delay-coordinate vector $\mathbf{z}$ at each step of the filter using the historical state variables from the open-loop run by,

$$\mathbf{z}_t = [\mathbf{x^o}_t, \mathbf{x^o}_{t-1}, \ldots, \mathbf{x^o}_{t-d}], \tag{23}$$

where d is the number of temporal delays. $\mathbf{x^o}$ contains the open-loop top, shallow and deep soil moisture, vegetation, snow, surface, and groundwater. Once the delay coordinate is created, the assimilation procedure can be applied. At each AUKF step, an ensemble of delay vectors is formed and advanced non-parametrically using a local approximation $\tilde{\mathbf{f}}$. This nonparametric prediction helps to build local models for predicting the dynamics at the forecast step (Hamilton et al., 2017). Given the above current delay-coordinate, the non-parametric advancement starts by locating the N nearest neighbors (i.e., points located within a given Euclidean distance; not only adjacent points), within a set of training data,

$$\begin{aligned}
\mathbf{z}_t^1 &= [\mathbf{x^o}^1_t, \mathbf{x^o}^1_{t-1}, \ldots, \mathbf{x^o}^1_{t-d}], \\
\mathbf{z}_t^2 &= [\mathbf{x^o}^2_t, \mathbf{x^o}^2_{t-1}, \ldots, \mathbf{x^o}^2_{t-d}], \\
&\vdots \\
\mathbf{z}_t^N &= [\mathbf{x^o}^N_t, \mathbf{x^o}^N_{t-1}, \ldots, \mathbf{x^o}^N_{t-d}].
\end{aligned} \tag{24}$$

The known $\mathbf{z}^1_{t+1}, \mathbf{z}^2_{t+1}, \ldots, \mathbf{z}^N_{t+1}$ (based on $\mathbf{x^o}^1_{t+1}, \mathbf{x^o}^2_{t+1}, \ldots, \mathbf{x^o}^N_{t+1}$), are used in a local model to predict $\mathbf{z}_{t+1}$. The local model $\tilde{\mathbf{f}}$, which can be generated using a weighted average of the nearest neighbors (Hamilton et al., 2016; Lagergren et al., 2018) can be written as,

$$\mathbf{z}_{t+1} = \omega_1 \mathbf{z}^1_{t+1} + \omega_2 \mathbf{z}^2_{t+1} + \ldots + \omega_N \mathbf{z}^N_{t+1}, \tag{25}$$

$$\omega_i = \frac{\mathrm{e}^{-(d_i/\sigma)^2}}{\sum_{j=1}^{N} \mathrm{e}^{-(d_j/\sigma)^2}}, \tag{26}$$

where d_i is the distance of the j^{th} neighbour to $\mathbf{z}_t$ and σ is a bandwidth parameter, which controls the contribution of each neighbor in the local model (here $\sigma = 2$). The above prediction is applied to estimate the delay coordinate vector at $t + 1$.

The process of building a local model for forecasting the delay-coordinate vector is repeated for each sigma point in the ensemble. After $\tilde{\mathbf{f}}$ has been defined, the remainder of the AUKF update scheme is implemented. Important to the Kalman-Takens method is the selection of d (the number of delays) and neighbors N. Here, we consider different values of N and d and set them based on the filter performance, which is described in Section 4. The assumption of using the model trajectory rather than observations for generating delay vectors allows us to reconstruct the system representing various water storage compartments. The same assumption is made by Lguensat et al. (2017), where trajectories of the system and not the physical model is available. In fact, we hypothesize that the available model outcomes can be used for the non-parametric sampling of the dynamics and updated by the GRACE TWS (as a summation of all the water variables at each grid point). This means that one can essentially correct state variables of the system, without having data for each individually, using the data-driven framework. The application of this method can address some severe limitations in traditional data assimilation such as large computational cost.

FIGURE 1

3.3. Synthetic experiment

A synthetic experiment is undertaken to assess the efficiency of the proposed data assimilation schemes in simulating physical processes. One important problem with hydrological models, and specifically W3RA, is their limitations in simulating anthropogenic impacts on the water cycle. For example, excessive groundwater extractions, which can largely affect sub-

surface water storages, are not modeled in W3RA and a successful data assimilation process should be able to correct for this drawback by taking the advantage of additional observations. Here, we choose to test both AUKF and Kalman-Takens filters to improve upon model simulations between 2003 and 2013 over Iran ($32.4279°N$, $53.6880°E$). The rationale behind choosing Iran for this synthetic analysis, and not Australia, is that a remarkable water storage decline is reported over this region, mainly due to anthropogenic impacts, which cannot be detected by W3RA (see Khaki et al., 2018b). A major part of the negative water storage trend is due to human impacts (see details in Forootan et al., 2017; Khaki et al., 2018b). Synthetic observations are produced using the WaterGAP Global Hydrology Model (WGHM; Döll et al., 2003; Müller et al., 2014) monthly TWS outputs, which contain the anthropogenic impacts (Khaki et al., 2018b), at two different spatial resolution of $1°\times1°$ and $3°\times3°$. This can help to test whether data assimilation can account for human impacts on water storage and also to investigate the effect of spatial resolution on the final results. WGHM TWS estimates are assumed as our observations after rescaling into $1°\times1°$ and $3°\times3°$ and perturbing using Monte Carlo sampling of multivariate normal distributions with the errors representing the GRACE level 2's standard errors. The data assimilation is implemented using both filtering methods at the aforementioned spatial scales.

3.4. Evaluation metrics

To evaluate the assimilation results against in-situ groundwater and soil moisture measurements, three metrics, (i) the Root-Mean-Squared Errors (RMSE), (ii) standard deviation (STD), and (iii) Nash-Sutcliffe coefficient (NSE) are used. Groundwater and soil moisture in-situ measurements from various stations are spatially averaged to the location of the nearest model grid points and are compared with their respective estimates. To this end, using the variation time series of in-situ data and the results of assimilation techniques, RMSE, STD, and NSE are calculated by,

$$RMSE = \sqrt{\frac{1}{n}\sum_{i=1}^{n}(x_i - z_i)^2}, \tag{27}$$

$$STD = \sqrt{\frac{1}{n}\sum_{i=1}^{n}(x_i - \bar{x})^2}, \tag{28}$$

$$NSE = 1 - \left[\frac{\sum_{i=1}^{n}(x_i - z_i)^2}{\sum_{i=1}^{n}(z_i - \bar{z})^2}\right], \tag{29}$$

where x_i is the predicted value (for n samples) and z_i represents the measured in-situ value. In Eqs. 27–29, $\bar{x}$ and $\bar{z}$ are the average of the predicted and measured values, respectively. Furthermore, to statistically assess the significance of the results, the student t-test is applied. The estimated t-value and the distribution at 0.05 significant level are used to calculate p-values.

4. Results

4.1. Synthetic experiment

The results of synthetic experiment, which is chosen to assess the capability of the two data assimilation schemes in improving model's simulation of physical processes are presented in this section. TWS variations from W3RA (open-loop; model integration without assimilation), AUKF and Kalman-Takens filters (with $N = 14$ and $d = 11$, see Section 4.2 for details), as well as synthetic observations, are displayed in Figure 2, where the time series represent spatially averaged TWS variations over the entire Iran. The trend lines corresponding to each time series are also depicted in the figure. As can be clearly seen, W3RA's open-loop run does not correctly capture the negative trend in the TWS time series as visible in the observations. Assimilation results, on the other hand, successfully reproduce the negative trend. Except for few cases, e.g., 2009 and 2011, Kalman-Takens performs closely to AUKF. The assimilation trend lines also show that the filtered results capture the existing trend of the observations. In addition to the trends, there are larger correlations between AUKF (14% on average) and Kalman-Takens (12% on average) with the observations compared to the open-loop results. An evaluation of the assimilation results against the original WGHM TWS, i.e., before perturbation using GRACE noises, are shown in Figure 3.

FIGURE 2

Figure 3 shows the scatter plot of the open-loop, AUKF, and Kalman-Takens TWS estimates against WGHM at the two spatial resolutions of $1^\circ \times 1^\circ$ and $3^\circ \times 3^\circ$ to assess the filters' performances at various spatial scales. Note that temporal assessment is also investigated in Section 4.2. It can be seen that at both spatial scales, there are larger agreements between the filtered results and WGHM. There are also smaller RMSEs after filtering, which suggests the capability of both methods to improve model simulations even in case of remarkable human impact. While every assimilation scenario leads to smaller RMSE than the open-loop run, the

least RMSEs are achieved at 1°×1° resolution. This shows that assimilating TWS observations at a finer resolution can provide better estimates regardless of the filtering method. It can also be seen that both AUKF and Kalman-Takens provide comparable results at both spatial scales, leading to approximately 48% RMSE reduction. The filters' comparable results at 3°×3° spatial resolution suggests their similar performance for downscaling TWS observations into the 1°×1° W3RA resolution.

FIGURE 3

4.2. Assessment with in-situ data

Independent groundwater and soil moisture in-situ measurements within the Murray-Darling Basin in Australia are used to evaluate the results. This is done by comparing the AUKF and Kalman-Takens estimates of groundwater and soil moisture with those of the in-situ measurements. Note that further analysis is undertaken to assess the impacts of the filters on non-assimilated variables and the results are provided in the supplementary material. Before comparing AUKF and Kalman-Takens results against in-situ measurements, we investigate the effect of various setups in the Kalman-Takens performance. Different scenarios are considered regarding the number of neighbors N (i.e., 2–40) and also the number of delays d (i.e., 1–25). To reach the best setup amongst these values, we compare the results of each scenario to the in-situ groundwater measurements. Figure 4 shows the average absolute groundwater errors resulting from each case. Increasing the number of neighbors can improve the approximation of training data for a particular point to a certain extent (due to the existing spatial correlations). However, selecting N too large can cause a rapid growth of errors, which is related to the effect of over-smoothing the training step. This is different for delays d, where much larger errors are present for smaller values that underestimate temporal variabilities in the data. From our numerical investigations, it can be seen that applying the Kalman-Takens filter with $N = 14$ and $d = 11$ provides the best result. It is worth mentioning that we use these setups of the Kalman-Takens filter throughout this study.

FIGURE 4

The comparison between the open-loop run, AUKF, and Kalman-Takens results are depicted in Figure 5, which displays scatter plot of each filter's RMSE and STD calculated using

in-situ groundwater measurements. Three different temporal evaluations are considered to further investigate the effect of temporal downscaling on the results. The GRACE TWS data (with approximately 30 days temporal scale) and associated errors are interpolated into a daily and 5-daily samples (see also Tangdamrongsub et al., 2015; Khaki et al., 2017b) using the spline interpolation between consecutive months. The assimilation is then undertaken on a daily, 5-day, and monthly basis. Figure 5 indicates that both AUKF and Kalman-Takens filters result in smaller RMSE and STD compared to the open-loop run for all the three temporal scales. In the daily and to a lesser degree 5-day assimilation cases, AUKF performs slightly better than the Kalman-Takens, with smaller RMSE and STD, which could be attributed to the contribution of the model equations for spreading TWS information between different variables after assimilation. Nevertheless, the performance of the non-parametric filter is satisfactory for both cases and comparable to that of AUKF. Interestingly, the performances of the two filters are even closer when assimilating monthly data. As a general result, this demonstrates that temporal downscaling of GRACE TWS data is recommended for data assimilation purpose regardless of the filtering method used. The average RMSE values for the 5-day assimilation using AUKF and Kalman-Takens filters are 51.28 ($\sim$13% smaller than daily and $\sim$7% smaller than monthly) and 53.61 ($\sim$16% smaller than daily and $\sim$5% smaller than monthly), respectively. Based on the above evaluation, it can be concluded that different temporal scales have similar effects on both filters, where the AUKF and Kalman-Takens filters perform better for the 5-day assimilation case.

FIGURE 5

More detailed statistics are provided in Table 1 to better compare the performances of the implemented filters against in-situ groundwater measurements. The evaluation is undertaken using RMSE and NSE metrics (see Section 3.4) based on the 5-day assimilation case. Note that in this table, basin-scale results are provided in addition to the results of the grid-based evaluation. Considering the coarse spatial resolution of W3RA and the fact that a number of groundwater stations can be found in each grid cell, basin-averaged assessment is performed as an alternative examination. The spatially averaged open-loop results and those from filters over the Murray-Darling Basin are tested against basin-average groundwater time series. Results of Table 1 confirm the behavior seen in Figure 5. While smaller RMSEs are obtained from AUKF

for both grid- and basin-based tests, the application of the Kalman-Takens method significantly decreases groundwater RMSE values (30.22% on average). Also larger NSE values are obtained by both filters compared to the open-loop run. These results prove a high capability of the Kalman-Takens for improving state estimates, very close to the AUKF performance. Table 1 also indicates that the Kalman-Takens approach can be used as traditional data assimilation to reduce noise in the final state variables, which are the results of solving complex inverse problems, e.g., groundwater estimates are improved from GRACE-derived TWS. This is also true for soil moisture estimates (cf. Table 2).

TABLE 1

We use different soil moisture layers from in-situ measurements including 0-8 cm (compared to the model top soil moisture layer), 0-30 cm (compared to the summation of the model top and shallow soil moisture layers), and 0-90 cm (compared to the summation of the model top, shallow, and deep soil moisture layers) for evaluating the results. Note that considering the difference between W3RA states (i.e., column water storage measured in mm) and the OzNet measurements (i.e., volumetric soil moisture) and the fact that converting the model outputs into volumetric units may introduce a bias (Renzullo et al., 2014), only NSE analysis is carried out and the results are provided in Table 2. Similar improvements as for groundwater evaluation are also found by comparing the filters estimates against OzNet soil moisture measurements (Table 2). Larger NSE values are found from data assimilation filters for all three soil layers. Average NSE from the Kalman-Takens method is 0.73, $\sim$12.3% larger than the open-loop run, and slightly smaller than AUKF results (0.74). Table 2 confirms that the capability of the Kalman-Takens method for improving the soil moisture estimates similar to AUKF (13.7% on average). The largest improvements for both filters are achieved in the root zone (0–90 cm) moisture layer. Table 2 suggests that AUKF better reflects the GRACE observations, especially at this layer. This, however, does not necessarily lead to better approximations in the shallow soil moisture layer, where the non-parametric approach shows higher improvements compared to AUKF.

TABLE 2

4.3. Assessing the performance of AUKF and Kalman-Taken filters

Here, we compare the performances of the AUKF and Kalman-Takens filters from various perspectives including increment applied, state covariance, computational efficiency, and water storage forecasting. Figure 6 shows the increments implemented by each filtering technique during the study period. We estimate average increment (i.e., ϵ discussed in Section 3.1) at all grid points for AUKF and the Kalman-Takens approach. One can see how the filters deal with the GRACE TWS observations in the update steps. Both methods decrease the increment as assimilation proceeds forward in time. This is found to be smaller for the Kalman-Takens method (see the trend lines in Figure 6) compared to AUKF. In fact, AUKF integrates the ensemble members through the model $\mathbf{f}$, while the non-parametric approach uses the local proxy $\tilde{\mathbf{f}}$. Consequently, larger misfits between the Kalman-Takens method forecast estimates and observations can be expected. Nevertheless, Figure 6 shows that the local proxy performs comparably to $\mathbf{f}$ in most of the time. In addition to increments, the difference between the filter's forecasting also affects the estimated error covariances, especially forecast covariance matrix (cf. Figure 7).

FIGURE 6

FIGURE 7

P_f and P_a are calculated at assimilation steps for both filters. The average of the matrices' diagonal elements are displayed in Figure 7. Despite the filters different performances in Figure 6, both methods perform very similar in dealing with the error covariances. The distribution of scattered error points from the Kalman-Takens filter and the corresponding trend line largely matches that of AUKF, which demonstrate that the filters have comparable uncertainty estimates. This indicates the ability of the Kalman-Takens method, which not only improves the model states but is also competitive with the traditional data assimilation system.

4.3.1. Filters efficiency

Computational complexity is important for data assimilation methods, especially when dealing with a high dimensional system, such as in hydrological studies. Therefore, a good data assimilation filter requires balancing between processes undertaken to achieve accurate estimates and computational efficiency. While the Kalman-Takens filter's capability for improving state

estimates have already been demonstrated (cf. Sections 4.1 and 4.2), its potential for decreasing the computational cost is examined here. This is done by comparing the computation time of the AUKF and Kalman-Takens filtering methods from various perspectives including forecasting, analysis steps, and filtering over the entire study period. Importantly, the following computation time estimates have been obtained using identical hardware. In the forecast step, the average computation time (for 794 grid points within Australia) is considerably lower for the Kalman-Takens filter, e.g., 6.12 second against 8.57 second for AUKF. This is due to the fact that the Kalman-Takens filter exploits the proxy model ($\tilde{f}$), which is based on a local approximation and requires much less computation than a physics-based model. The average computational time at the analysis steps is 5.74 second for the Kalman-Takens filter and 7.83 seconds for AUKF. Considering that both methods are using similar analysis filtering, this difference is due to the local scheme (based on d delays and N neighbor points) in the Kalman-Takens method. The values of delays d and neighbors N determine the number of local points used in the analysis and accordingly the size of the underlying vectors and matrices. AUKF, on the other hand, solves for all grid points altogether, which requires a larger amount of memory and time. In general, it is found that the Kalman-Takens is considerably less computationally demanding, i.e., ~ 8 times faster for the entire experiment period, compared to the AUKF implementation for assimilating all observations into the system states.

4.3.2. Water storage update

In this section, we analyze the spatio-temporal increments derived by assimilating the GRACE TWS observations and explore their effects on the states. Figure 8 presents the average TWS time series after applying each filter, open-loop, and GRACE observations over Australia. Both filters largely decrease the misfits between the model states and the GRACE observations, which is expected since GRACE is used as a constraint. AUKF, however, has a larger impact on the states, especially where a significant TWS variation exists (e.g., 2006 and 2011–2012). The Kalman-Takens method, on the other hand, shows a smoother time series. Based on these results, we find that the Kalman-Takens approach is able to efficiently integrate observations into the model and correct missing trends as well as amplitudes and phases. Nevertheless, one can conclude that this method might not be able to efficiently extract spontaneous or high rate seasonal effects unless the training data has these variabilities/dynamics.

FIGURE 8

The correlation between the estimated TWS time series from the open-loop model run and the filters' estimates at each grid point within Australia and those of the GRACE TWS are presented in Figure 9. The filters largely increase the correlation between model derived TWS and those of GRACE. The largest correlations (with 0.92 average) is obtained by AUKF suggesting that this method better reflects the GRACE TWS into the states. The average correlation between TWS of the Kalman-Takens and GRACE is 0.89 (0.03 less than AUKF), and when compared to only 0.52 obtained from the open-loop estimates, the efficiency of the method becomes visible. Correlations of the open-loop TWS and GRACE are smaller over the mountainous area along the East coast compared to other parts of the country. This is due to difficulties of modeling hydrology in complex terrain areas (mountains). On the other hand, both assimilation methods show good performances by increased correlations with GRACE data. Over large parts of Australia, the performances of the Kalman-Takens filter and AUKF are found to be similar in terms of correlations with the GRACE TWS.

FIGURE 9

To further assess the capability of the filtering approaches for improving the model simulations, we test their ability in correcting the model variables for extreme and poorly known hydrological phenomena. To this end, the filters' TWS results are monitored between 2003 and 2012 over the Murray-Darling Basin. As shown by Schumacher et al. (2018), a long-term drought period (2001–2009), known as Millennium Drought (e.g., Ummenhofer et al., 2009; LeBlanc et al., 2012; van Dijk et al., 2013), has remarkably affected TWS variations in the basin. This negative TWS trend has then been followed by an above average precipitation, mainly caused by El Niño Southern Oscillation (ENSO; see, e.g., Boening et al., 2012; Forootan et al., 2016) for the period of 2010–2012. Here, we investigate the capability of the open-loop, AUKF, and Kalman-Takens TWS estimates to capture these two extreme events. Figure 10 plots the average TWS time series of the above methods, as well as GRACE-derived TWS over the Murray-Darling Basin. As can be seen, while both Millennium drought (red shaded area) and ENSO effect (blue shaded area) are reflected in GRACE TWS time series, the open-loop run is unable to capture them, especially the drought effects. AUKF and the Kalman-Takens

filter, on the other hand, successfully depict the negative trend between 2003 and 2010, followed by a positive anomaly after 2010. Except for few points such as 2004, 2007, and late 2009, the Kalman-Takens method presents a similar performance as AUKF in incorporating GRACE TWS data with states and reflecting extreme hydrological events.

FIGURE 10

5. Conclusions

The present study investigates the ability of the Kalman-Takens approach to reconstruct the nonlinear dynamics of a hydrological model. This is done to update observable state variables based on new observations when a physics-based model is not available. This implies that contrary to a standard data assimilation, the Kalman-Takens filter does not affect non-observed variables (e.g., water discharge in our case). In this work, we introduce a new setup for the Kalman-Takens filter to reconstruct additional states (e.g., soil moisture and groundwater) using the Gravity Recovery And Climate Experiment (GRACE) terrestrial water storage (TWS). The Kalman-Takens results are compared with a parametric forecasting approach of an adaptive unscented Kalman filtering (AUKF) as well as against in-situ groundwater and soil moisture measurements. The results prove a high capability of the Kalman-Takens for improving state estimates, largely comparable to the AUKF performance and as such, both provide efficient methods for assimilating GRACE TWS data. Results indicate that smaller RMSE (46.96 mm) and higher NSE (0.82) values are obtained from the application of the Kalman-Takens method in comparison to the open-loop run (69.40 mm RMSE and 0.58 NSE). Although AUKF performs slightly better in some cases, e.g., $\sim$3% higher improvement for groundwater estimates, which is expected since AUKF takes advantage of the full knowledge of the model while the non-parametric filter uses only the short noisy training data set from which to learn the dynamics, in all cases considered, the Kalman-Takens results are generally very close to those of AUKF. The data-driven approach also increases the NSE values between the estimated soil moisture variations and the OzNet in-situ measurements for all soil layers (11.83% on average) as compared to AUKF (13.77% on average). The proposed approach also reduces estimation complexities by using the local proxy model. The Kalman-Takens filter performs more efficient ($\sim$ 8 times faster) in terms of computational cost, which is very important to deal with a growing amount of data sets in high dimensional systems. This contribution, to the best of the

authors' knowledge, is the first effort in using the data-driven approach in hydrological studies with complex state observation transition systems. Further research should be undertaken to investigate the Kalman-Takens filter in different hydrological applications and also to explore its capability in dealing with multiple satellite products.

6. Acknowledgement

We would like to thank Tyrus Berry and Timothy Sauer for their valuable help in this study. M. Khaki is grateful for the research grant of Curtin International Postgraduate Research Scholarships (CIPRS)/ORD Scholarship provided by Curtin University (Australia). F. Hamilton is supported by National Science Foundation grant No. RTG/DMS-1246991. This work is a TIGeR publication. The GRACE data are acquired from the ITSG-Grace2014 gravity field model (Mayer-Gürr et al., 2014). In-situ groundwater and soil moisture measurements are obtained from the New South Wales Government (NSW; http://waterinfo.nsw.gov.au/pinneena/gw.shtml) and the OzNet network (http://www.oznet.org.au/), respectively. Meteorological forcing data are provided by Princeton University (http://hydrology.princeton.edu). Other data used in this study can be found at DOI: 10.6084/m9.figshare.5942548. A more detailed discussion of the results can be found in the supporting information (Huffman et al., 2007; Mu et al., 2011).

References

References

Alsdorf, D.E., Rodriguez, E., Lettenmaier, D.P., (2007). Measuring surface water from space, Rev. Geophys., 45, RG2002, http://dx.doi.org/10.1029/2006RG000197.

Andreadis, K.M., Clark, E.A., Lettenmaier, D.P., Alsdorf, D.E., (2007). Prospects for river discharge and depth estimation through assimilation of swathaltimetry into a raster-based hydrodynamics model. Geophysical Research Letters 34: http://dx.doi.org/10.1029/2007GL02972.

Arnold, H., Moroz, I., Palmer, T., (2013). Stochastic Parametrizations and Model Uncertainty in the Lorenz '96 System, Phil. Trans. R. Soc. A 371, 20110479.

Awwad, H.M., Valdés, J.B., Restrepo, P.J., (1994). Streamflow forecasting for Han River basin, Korea. J. Water Resour. Plann. Manage., 120, 651–673.

Bennett, A.F., (2002); Inverse Modeling of the Ocean and Atmosphere, 234 pp., Cambridge Univ. Press, New York.

Berry, T., Sauer, T., (2013). Adaptive ensemble Kalman filtering of non-linear, Tellus A: Dynamic Meteorology and Oceanography, Volume 65, Issue 1, Article: 20331, http://dx.doi.org/10.3402/tellusa.v65i0.20331.

Berry, T., Harlim, J., (2016). Variable Bandwidth Diffusion Kernels, Appl. Comput. Harmon. Anal., 40, 68.

Boening, C., Willis, J.K., Landerer, F.W., Nerem, R.S., Fasullo, J., (2012). The 2011 La Niña: so strong, the oceans fell. Geophys. Res. Lett. 39, L19602. http://dx.doi.org/10.1029/2012GL053055.

BoM, (2010). Australian Rainfall Patterns During El Niño Events. Bureau of Meteorology. Accessed at http://www.bom.gov.au/climate/enso/ninocomp.shtml.

Botterill, L.C., (2003). Uncertain Climate: The Recent History of Drought Policy in Australia. Australian Journal of Politics & History, 49: 61–74, http://dx.doi.org/10.1111/1467-8497.00281.

Bras, R.L., Restrepo-Posada, P., (1980). Real time automatic parameter calibration in conceptual runoff forecasting models. Proc. Third Int. Symp. on Stochastic Hydraulics, 61–70.

Brocca, L., Melone, F., Moramarco, T., Wagner, W., Naeimi, V., Bartalis, Z., Hasenauer, S., (2010). Improving runoff prediction through the assimilation of the ASCAT soil moisture product, Hydrol. Earth Syst. Sci., 14, 1881–1893, http://dx.doi.org/10.5194/hess-14-1881-2010.

Calvet, J.-C., Noilhan, J., Bessemoulin, P., (1998). Retrieving root-zone soil moisture from surface soil moisture of temperature estimates: A feasibility study based on field measurements. J. Appl. Meteor., 37, 371–386.

Cheng, M.K., Tapley, B.D., (2004). Variations in the Earth's oblateness during the past 28 years. Journal of Geophysical Research, Solid Earth, 109, B09402. http://dx.doi.org/10.1029/2004JB003028.

580 Chiew, F.H.S., Stewardson, M.J., McMahon, T.A., (1993). Comparison of six rainfall-runoff
581 modelling approaches, J. Hydrol., 147, 1–36.

582 Christiansen, L., Krogh, P.E., Bauer-Gottwein, P., Andersen, O.B., Leiriäo, S., Binning, P.J.,
583 Rosbjerg, D., (2007). Local to regional hydrological model calibration for the Okavango
584 River Basin from In-situ and space borne gravity observations. Proceedings of 2nd Space for
585 Hydrology Workshop, Geneva, Switzerland, 12-14.

586 Coumou, D., Rahmstorf, S., (2012). A decade of weather extremes Nat. Clim. Change, 2 (7),
587 pp. 1–6.

588 CSIRO, BoM, (2014). State of the Climate 2014. CSIRO and Bureau of Meteorology, Melbourne.

589 CSIRO, BoM, (2015). Climate change in Australia: Projections for Australia's NRM regions.
590 Technical Report, 216pp.

591 De Lannoy, G., Pauwels, V.R.N., Houser, P.R., Verhoest, N.E.C., Gish, T., (2007). Repre-
592 sentativeness of point soil moisture observations, upscaling and assimilation. IUGG General
593 Assembly, Perugia Italy, Session HS2004, July 2-13.

594 De Lannoy, G.J.M., Reichle, R.H., Houser, P.R., Pauwels, V.R.N., Verhoes, N.E.C., (2007).
595 Correcting for forecast bias in soil moisture assimilation with the ensemble Kalman filter.
596 Water Resour. Res. 43, W09410, http://dx.doi.org/10.1029/2006WR00544.

597 De Lannoy, G.J.M., Houser, P.R., Pauwels, V.R.N., Verhoest, N.E., (2009). Assessment of model
598 uncertainty for soil moisture through ensemble verification. J. Geophys. Res. 111, D10101,
599 http://dx.doi.org/10.1029/2005JD006367

600 De Lannoy, G.J.M., de Rosnay, P., Reichle, R.H., (2015). Soil Moisture Data Assimilation. In:
601 Duan Q., Pappenberger F., Thielen J., Wood A., Cloke H., Schaake J. (eds) Handbook of
602 Hydrometeorological Ensemble Forecasting. Springer, Berlin, Heidelberg.

603 DFAT (Department of Foreign Affairs and Trade) (2014). DFAT Annual Report, DFAT, Can-
604 berra.

605 Döll, P., Kaspar, F., Lehner, B., (2003). A global hydrological model for deriving water avail-
606 ability indicators: model tuning and validation, J. Hydrol., 270, 105–134.

607 Dreano, D., Mallick, B., Hoteit, I., (2015). Filtering remotely sensed chlorophyll concentrations
608 in the Red Sea using a space–time covariance model and a Kalman filter, Spatial Statistics,
609 Volume 13, Pages 1-20, ISSN 2211-6753, http://dx.doi.org/10.1016/j.spasta.2015.04.002.

610 Entekhabi, D., Nakamura, H., Njoku, E.G., (1994). Solving the inverse problem for soil mois-
611 ture and temperature profiles by sequential assimilation of multifrequency remotely senses
612 observations. IEEE Trans. Geosci. Remote Sens., 32, 438–448.

613 Eicker, A., Schumacher, M., Kusche, J., Döll, P., Müller-Schmied, H., (2014). Calibra-
614 tion/data assimilation approach for integrating GRACE data into the WaterGAP global
615 hydrology model (WGHM) using an ensemble Kalman filter: first results, SurvGeophys,
616 35(6):1285–1309. http://dx.doi.org/10.1007/s10712-014-9309-8.

617 Elbern, H., Schmidt, H., (2001). Ozone episode analysis by fourdimensional variational chem-
618 istry data assimilation, J. Geophys. Res., 106, 3569–3590.

619 Famiglietti, J.S., Ryu, D., Berg, A.A., Rodell, M., Jackson, T.J., (2008). Field ob-
620 servations of soil moisture variability across scales, Water Resour. Res., 44, W01423,
621 http://dx.doi.org/10.1029/2006WR005804.

622 Forootan, E., Khandu, Awange, J., Schumacher, M., Anyah, R., van Dijk, A., Kusche, J.,
623 (2016). Quantifying the impacts of ENSO and IOD on rain gauge and remotely sensed
624 precipitation products over Australia. Remote Sensing of Environment,172, Pages 50-66,
625 http://dx.doi.org/10.1016/j.rse.2015.10.027.

626 Forootan, E., Safari, A., Mostafaie, A., Schumacher, M., Delavar, M., Awange, J., (2017).
627 Large-Scale Total Water Storage and Water Flux Changes over the Arid and Semiarid Parts
628 of the Middle East from GRACE and Reanalysis Products. Surveys in Geophysics 38(3), pp.
629 591-615, http://dx.doi.org/10.1007/s10712-016-9403-1.

630 Girotto, M., De Lannoy, G.J.M,. Reichle, R.H., Rodell, M., (2016). Assimilation of gridded
631 terrestrial water storage observations from GRACE into a land surface model, Water Resour.
632 Res., 52, 4164–4183, http://dx.doi.org/10.1002/2015WR018417.

633 Girotto, M., De Lannoy, G.J.M., Reichle, R.H., Rodell, M., Draper, C., Bhanja, S.N.,
634 Mukherjee, A., (2017). Benefits and pitfalls of GRACE data assimilation: A case study

635 of terrestrial water storage depletion in India, Geophys. Res. Lett., 44, 4107–4115,
636 http://dx.doi.org/10.1002/2017GL072994.

637 Giustarini, L., Matgen, P., Hostache, R., Montanari, M., Plaza, D., Pauwels, V.R.N., De Lan-
638 noy, G.J.M., De Keyser, R., Pfister, L., Hoffmann, L., Savenije, H.H.G., (2011). Assimilating
639 SAR-derived water level data into a hydraulic model: a case study, Hydrol. Earth Syst. Sci.,
640 15, 2349–2365, http://dx.doi.org/10.5194/hess-15-2349-2011.

641 Hamilton, F., Berry, T., Sauer, T., (2015), Pred icting Chaotic Time Series with a Partial
642 Model, Phys. Rev. E 92, 010902.

643 Hamilton, F., Berry, T., Sauer, T., (2016). Ensemble Kalman Filtering without a Model, Phys.
644 Rev. X 6, 011021, Vol. 6, Iss. 1, http://dx.doi.org/10.1103/PhysRevX.6.011021.

645 Hamilton, F., Berry, T., Sauer, T., (2017). Kalman-Takens filtering in the presence of dynamical
646 noise, *To appear, Eur. Phys. J: ST.*

647 Harris, I.C., (2008). Climatic Research Unit (CRU) time-series datasets of variations in
648 climate with variations in other phenomena. NCAS British Atmospheric Data Cen-
649 tre, date of citation, University of East Anglia Climatic Research Unit; Jones, P.D.,
650 http://catalogue.ceda.ac.uk/uuid/3f8944800cc48e1cbc29a5ee12d8542d.

651 Hersbach, H., Stoffelen, A., De Haan, S., (2007). An Improved C-Band Scatterometer Ocean
652 Geophysical Model Function: CMOD5, J. Geophys. Res. Oceans 112, C03006.

653 Hoteit, I., Pham, D.T., Blum, J., (2002). A simplified reducedorder kalman filtering and appli-
654 cation to altimetric data assimilation in tropical Pacific. J. Mar. Syst., 36, 101–127.

655 Hoteit, I., Luo, X., Pham, D.T., (2012). Particle Kalman Filtering: A Nonlinear Bayesian
656 Framework for Ensemble Kalman Filters, Monthly Weather Review, 140:2, 528-542.

657 Huang, S., Kumar, R., Flörke, M., Yang T., Hundecha, Y., Kraft, P., Gao, C., Gelfan, A., Lier-
658 sch, S., Lobanova, A., Strauch, M., Ogtrop, F.V., Reinhardt, J., Haberlandt, U., Krysanova,
659 V., (2016). Evaluation of an ensemble of regional hydrological models in 12 large-scale river
660 basins worldwide. Clim Chang. http://dx.doi.org/10.1007/s10584-016-1841-8.

661 Huffman, G.J., Adler, R.F., Bolvin, D.T., Gu, G., Nelkin, E.J., Bowman, K.P., Hong, Y.,
662 Stocker, E.F., Wolff, D.B., (2007). The TRMM Multi-satellite Precipitation Analysis: Quasi-

663 Global, Multi-Year, Combined-Sensor Precipitation Estimates at Fine Scale. J. Hydrometeor.,
664 8(1), 38-55.

665 Huntington, T.G., (2006). Evidence for intensification of the global water cycle: Review and
666 synthesis, J. Hydrol.,319(1–4), 83–95, http://dx.doi.org/10.1016/j.jhydrol.2005.07.003.

667 Irmak, A., Kamble, B., (2009). Evapotranspiration data assimilation with genetic algorithms
668 and SWAP model for on-demand irrigation. Irrigation Science, 28(1): 101–112.

669 Julier, S.J., Uhlmann, J.K., (1997). A New Extension of the Kalman Filter to Nonlinear Sys-
670 tems. In Proc. of AeroSense: The 11th Int. Symp. on Aerospace/Defence Sensing, Simulation
671 and Controls.

672 Julier, S., Uhlmann, J., Durrant-Whyte, H.F., (2000). A new method for the nonlinear trans-
673 formation of means and covariances in filters and estimators, IEEE Trans. Automat. Control
674 45, 477-482.

675 Julier, S.J. and Uhlmann, J.K., (2004). Unscented filtering and nonlinear estimation, Proc.
676 IEEE 92, 401-422.

677 Kalnay, E., (2003). Atmospheric modelling, data assimilation and predictability, Cam-
678 bridge University Press. pp. xxii 341. ISBNs 0 521 79179 0, 0 521 79629 6,
679 http://dx.doi.org/10.1256/00359000360683511.

680 Kiem, A.S., Johnson, F., Westra, S., van Dijk, A., Evans, J.P., O'Donnell, A., Rouil-
681 lard, A., Barr, C., Tyler, J., Thyer, M., Jakob, D., Woldemeskel, F., Sivakumar,
682 B., Mehrotra, R., (2016). Natural hazards in Australia: droughts. Clim. Change.
683 http://dx.doi.org/10.1007/s10584-016-1798-7.

684 Khaki, M., Hoteit, I., Kuhn, M., Awange, J., Forootan, E., van Dijk, A.I.J.M., Schumacher,
685 M., Pattiaratchi, C., (2017a). Assessing sequential data assimilation techniques for integrating
686 GRACE data into a hydrological model, Advances in Water Resources, Volume 107, Pages
687 301-316, ISSN 0309-1708, http://dx.doi.org/10.1016/j.advwatres.2017.07.001.

688 Khaki, M., Schumacher, M., J., Forootan, Kuhn, M., Awange, E., van Dijk, A.I.J.M., (2017b).
689 Accounting for Spatial Correlation Errors in the Assimilation of GRACE into Hydrological
690 Models through localization, Advances in Water Resources, Available online 1 August 2017,
691 ISSN 0309-1708, https://doi.org/10.1016/j.advwatres.2017.07.024.

692 Khaki, M., Ait-El-Fquih, B., Hoteit, I., Forootan, E., Awange, J., Kuhn, M., (2017c). A two-
693 update ensemble Kalman filter for land hydrological data assimilation with an uncertain
694 constraint, In Journal of Hydrology, Volume 555, 2017, Pages 447-462, ISSN 0022-1694,
695 https://doi.org/10.1016/j.jhydrol.2017.10.032.

696 Khaki, M., Forootan, E., Kuhn, M., Awange, J., Papa, F., Shum, C.K., (2018a). A Study of
697 Bangladesh's Sub-surface Water Storages Using Satellite Products and Data Assimilation
698 Scheme, accepted in Advances in Water Resources.

699 Khaki, M., Forootan, E., Kuhn, M., Awange, J., van Dijk, A.I.J.M., Schumacher, M., Sharifi,
700 M.A., (2018b). Determining Water Storage Depletion within Iran by Assimilating GRACE
701 data into the W3RA Hydrological Model, Advances in Water Resources, 114:1-18,

702 Khaki, M., Forootan, E., Kuhn, M., Awange, J., Longuevergne, L., Wada, W., (2018c). Ef-
703 ficient Basin Scale Filtering of GRACE Satellite Products, In Remote Sensing of Environ-
704 ment, Volume 204, Pages 76-93, ISSN 0034-4257, https://doi.org/10.1016/j.rse.2017.10.040.
705 https://doi.org/10.1016/j.advwatres.2018.02.008.

706 Kumar, S.V., Reichle, R.H., Koster, R.D., Crow, W.T., Peters-Lidard, C.D., (2009). Role of
707 subsurface physics in the assimilation of surface soil moisture observations. J. Hydromet. 10
708 (6), 1534–1547. http://dx.doi.org/10.1175/2009JHM1134.1.

709 Kumar, S.V., Peters-Lidard, C.D., Santanello, J.A., Reichle, R.H., Draper, C.S., Koster,
710 R.D., Nearing, G., Jasinski, M.F., (2015). Evaluating the utility of satellite soil mois-
711 ture retrievals over irrigated areas and the ability of land data assimilation methods to
712 correct for unmodeled processes, Hydrology and Earth System Sciences, 19, 4463-4478,
713 http://dx.doi.org/10.5194/hess-19-4463-2015.

714 Kumar, S., Zaitchik, B., Peters-Lidard, C., Rodell, M., Reichle, R., Li, B., Jasinski, M.,
715 Mocko, D., (2016). Assimilation of Gridded GRACE Terrestrial Water Storage Estimates
716 in the North American Land Data Assimilation System. J. Hydrometeor., 17, 1951–1972,
717 http://dx.doi.org/10.1175/JHM-D-15-0157.1.

718 Kusche, J., Schmidt R., Petrovic, S., Rietbroek, R., (2009). Decorrelated GRACE time-variable
719 gravity solutions by GFZ and their validation using a hydrological model, Journal of Geodesy,
720 DOI 10.1007/s00190-009-0308-3.

Lahoz, W.A., Geer, A.J., Bekki, S., Bormann, N., Ceccherini, S., Elbern, H., Errera, Q., Eskes, H.J., Fonteyn, D., Jackson, D.R., Khattatov, B., (2007). The Assimilation of Envisat data (ASSET) project, Atmos. Chem. Phys., 7, 1773 - 1796.

Lagergren, J., Reeder, A., Hamilton, F., Smith, R.C., Flores, K.B., (2018). Forecasting and Uncertainty Quantification Using a Hybrid of Mechanistic and Non-mechanistic Models for an Age-Structured Population Model, Bull Math Biol, https://doi.org/10.1007/s11538-018-0421-7.

Botterill, L.C., Fisher, M., (2012). Beyond Drought: People, Policy and Perspectives, CSIRO Publishing, Melbourne, DAFF (Department of Agriculture, Fisheries and Forestry), Drought and Natural Disaster Declaration: 12 September. Queensland Government. Accessed at https://www.longpaddock.qld.gov.au/queenslanddroughtmonitor/queenslanddroughtreport/.

LeBlanc, M., Tweed, S., Van Dijk, A., Timbal, B., (2012). A review of historic and future hydrological changes in the Murray Darling Basin. Global Planetary Change (80–81): 226–246.

Lee, H., Seo, D.-J., Koren, V., (2011). Assimilation of streamflow and in situ soil moisture data into operational distributed hydrologic models: Effects of uncertainties in the data and initial model soil moisture states, Adv. Water Resour., 34(12), 1597–1615, http://dx.doi.org/10.1016/j.advwatres.2011.08.012.

Lguensat, R., Tandeo, P., Ailliot, P., Pulido, M., Fablet, R., (2017). The Analog Data Assimilation. Mon. Wea. Rev., https://doi.org/10.1175/MWR-D-16-0441.1.

Li, Y., Ryu, D., Western, A.W., Wang, Q.J., (2015). Assimilation of stream discharge for flood forecasting: Updating a semidistributed model with an integrated data assimilation scheme, Water Resour. Res., 51, 3238–3258, http://dx.doi.org/10.1002/2014WR016667.

Lievens, H., Kumar, S., Al Bitar, A., De Lannoy, G.J.M., Drusch, M., Dumedah, G., Hendricks Franssen, H.J., Kerr, Y.H., Martens, B., Pan, M., Roundy, J.K., Vereecken, H., Walker, J.P., Wood, E.F., Verhoest, N.E.C., Pauwels, V.R.N., (2015). SMOS soil moisture assimilation for improved hydrologic simulation in the Murray Darling Basin, Australia, Remote Sensing of Environment, 168(10), 146–162.

Madsen, H., Skotner, C., (2005). Adaptive state-updating in real-time river flow forecasting—A combined filtering and error forecasting procedure. J. Hydrol., 308, 302–312.

Mayer-Gürr, T., Zehentner, N., Klinger, B., Kvas, A., (2014). ITSG-Grace2014: a new GRACE gravity field release computed in Graz. - in: GRACE Science Team Meeting (GSTM), Potsdam am: 29.09.2014.

McMillan, H.K., Hreinsson, E.Ö., Clark, M.P., Singh, S.K., Zammit, C., Uddstrom, M.J., (2013). Operational hydrological data assimilation with the recursive ensemble Kalman filter, Hydrol. Earth Syst. Sci., 17(1), 21–38, http://dx.doi.org/10.5194/hess-17-21-2013.

Mehra, R., (1970). On the identification of variances and adaptive Kalman filtering. IEEE Trans. Auto. Cont. 15, 175-184.

Mehra, R., (1972). Approaches to adaptive filtering. IEEE Trans. Auto. Cont. 17, 693-698.

Mercer, D., Christesen, L., Buston, M., (2007). Squandering the future—Climate change, policy failure and the water crisis in Australia. Futures 39: 272–287.

Montaldo, N., Albertson, J.D., Mancini, M., Kiely, G., (2001). Robust simulation of root zone soil moisture with assimilation of surface soil moisture data. Water Resour. Res., 37, 2889–2900.

Mu, Q., Zhao, M., Running, S.W., (2011). Improvements to a MODIS Global Terrestrial Evapotranspiration Algorithm. Remote Sensing of Environment 115: 1781-1800.

Müller Schmied, H., S. Eisner, D. Franz, M. Wattenbach, F. Portmann, M. Flörke, Döll, P., (2014). Sensitivity of simulated global-scale freshwater fluxes and storages to input data, hydrological model structure, human water use and calibration, Hydrol. Earth. Syst. Sci., 18, 3511–3538, http://dx.doi.org/10.5194/hess-18-3511-2014.

Neal, J., Schumann, G., Bates, P., Buytaert, W., Matgen, P., Pappenberger, F., (2009). A data assimilation approach to discharge estimation from space, Hydrol. Process., 23, 3641–3649.

Nicolai-Shaw, N., Hirschi, M., Mittelbach, H., Seneviratne, S.I., (2015). Spatial representativeness of soil moisture using in situ, remote sensing, and land reanalysis data, J. Geophys. Res. Atmos., 120, 9955–9964, http://dx.doi.org/10.1002/2015JD023305.

Orlowsky, B., Seneviratne, S.I., (2014). On the spatial representativeness of temporal dynamics at European weather stations, Int. J. Climatol., 34(10), 3154–3160, http://dx.doi.org/10.1002/joc.3903.

778 Packard, N.H., Crutchfield, J.P., Farmer, J.D., Shaw, R.S., (1980). Geometry from a Time
779 Series, Phys. Rev. Lett. 45, 712.

780 Palmer, T.N., (2001). A Nonlinear Dynamical Perspective on Model Error: A Proposal for
781 Non-Local Stochastic-Dynamic Parametrization in Weather and Climate Prediction Models,
782 Q. J. R. Meteorol. Soc. 127, 279.

783 Pipunic, C., Walker, P., Western, A., (2008). Assimilation of remotely sensed data for improved
784 latent and sensible heat flux prediction: A comparative synthetic study. Remote Sensing of
785 Environment, 112(4): 1295–1305.

786 Rasmussen, J., Madsen, H., Jensen, K.H., and Refsgaard, J.C., (2015). Data assimilation in
787 integrated hydrological modeling using ensemble Kalman filtering: evaluating the effect of
788 ensemble size and localization on filter performance, Hydrol. Earth Syst. Sci., 19, 2999-3013,
789 https://doi.org/10.5194/hess-19-2999-2015.

790 Reager, J.T., Thomas, A.C., Sproles, E.A., Rodell, M., Beaudoing, H.K., Li, B., Famiglietti,
791 J.S., (2015). Assimilation of GRACE Terrestrial Water Storage Observations into a Land
792 Surface Model for the Assessment of Regional Flood Potential. Remote Sens. 2015, 7, 14663-
793 14679.

794 Reichle, R.H., McLaughlin, D.B., Entekhabi, D., (2002). Hydrologic Data Assimilation with
795 the Ensemble Kalman Filter. Mon. Wea. Rev. 130, 103–114, http://dx.doi.org/10.1175/1520-
796 0493(2002)130¡0103:HDAWTE¿2.0.CO;2.

797 Reichle, R.H., Koster, R.D., (2005). Global Assimilation of Satellite Surface Soil Moisture
798 Retrievals into the NASA Catchment Land Surface Model, Geophys. Res. Lett. 32, L02404.

799 Renzullo, L.J., Van Dijk, A.I.J.M., Perraud, J.M., Collins, D., Henderson, B., Jin, H., Smith,
800 A.B., McJannet, D.L., (2014). Continental satellite soil moisture data assimilation improves
801 root-zone moisture analysis for water resources assessment. J. Hydrol., 519, 2747–2762.
802 http://dx.doi.org/10.1016/j.jhydrol.2014.08.008.

803 Rodell, M., Chen, J., Kato, H., Famiglietti, J.S., Nigro, J., Wilson, C.R., (2007). Estimating
804 groundwater storage changes in the Mississippi River basin (USA) using GRACE, Hydrogeol.
805 J., 15, 159–166.

Sauer, T., Yorke, J., Casdagli, M., (1991). Embedology, J. Stat. Phys. 65, 579.

Sauer, T., (2004). Reconstruction of Shared Nonlinear Dynamics in a Network, Phys. Rev. Lett. 93, 198701.

Schumacher, M., Kusche, J., Döll, P., (2016). A systematic impact assessment of GRACE error correlation on data assimilation in hydrological models, Journal of Geodesy, http://dx.doi.org/10.1007/s00190-016-0892-y.

Schumacher, M., Forootan, E., van Dijk, A.I.J.M., Müller Schmied, H., Crosbie, R.S., Kusche, J., Döll, P., (2018). Improving drought simulations within the Murray-Darling Basin by combined calibration/assimilation of GRACE data into the WaterGAP Global Hydrology Model, In Remote Sensing of Environment, Volume 204, Pages 212-228, ISSN 0034-4257, https://doi.org/10.1016/j.rse.2017.10.029.

Schunk, R.W., Scherliess, L., Sojka, J.J., Thompson, D.C., (2004). USU global ionospheric data assimilation models, Atmospheric and Environmental Remote Sensing Data Processing and Utilization: an End-to-End System Perspective, (ed. H.-L. A. Huang and H. J. Bloom), Proc. of SPIE, 5548, http://dx.doi.org/10.1117/12.562448, 327-336.

Schuurmans, M., Troch A., Veldhuizen, A., et al., (2003). Assimilation of remotely sensed latent heat flux in a distributed hydrological model. Advances in Water Resources, 26(2): 151–159.

Seo, D.J., Koren, V., Cajina, N., (2003). Real-time variational assimilation of hydrologic and hydrometeorological data into operational hydrologic forecasting. J. Hydrometeorol., 4, 627–641.

Seoane, L., Ramillien, G., Frappart, F., Leblanc, M., (2013). Regional GRACE-based estimates of water mass variations over Australia: validation and interpretation, Hydrol. Earth Syst. Sci., 17, 4925-4939, http://dx.doi.org/10.5194/hess-17-4925-2013.

Sheffield, J., Goteti, G., Wood, E. F., (2006). Development of a 50-yearhigh-resolution global dataset of meteorological forcings for land surfacemodeling, J. Clim., 19(13), 3088–3111.

Simon, D., (2006). Optimal state estimation: Kalman, H_∞, and nonlinear approaches, John Wiley and Sons.

Smith, P.J., Dance, S.L., Nichols, N.K., (2011). A hybrid data assimilation scheme for model parameter estimation: Application to morphodynamic modelling, Comput-

834 ers and Fluids, Volume 46, Issue 1, July 2011, Pages 436-441, ISSN 0045-7930,
835 http://dx.doi.org/10.1016/j.compfluid.2011.01.010.

836 Song, Q., He, Y., (2009). Adaptive unscented Kalman filter for estimation of modelling errors for
837 helicopter, IEEE International Conference on Robotics and Biomimetics (ROBIO), Guilin,
838 2009, pp. 2463-2467, http://dx.doi.org/10.1109/ROBIO.2009.5420406.

839 Swenson, S., Chambers, D., Wahr, J., (2008). Estimating geocentervariations from a combi-
840 nation of GRACE and ocean model output. Journal of Geophysical research, 113, B08410,
841 http://dx.doi.org/10.1029/2007JB005338.

842 Takens, F., (1981). Dynamical Systems and Turbulence, Warwick 1980, Lect. Notes Math. 898,
843 366.

844 Tandeo, P., Coauthors, (2015). Combining analog method and ensemble data assimilation:
845 application to the lorenz-63 chaotic system. Machine Learning and Data Mining Approaches
846 to Climate Science, Springer, 3–12.

847 Tangdamrongsub, N., Steele-Dunne, S.C., Gunter, B.C., Ditmar, P.G., and Weerts, A.H.,
848 (2015). Data assimilation of GRACE terrestrial water storage estimates into a regional
849 hydrological model of the Rhine River basin, Hydrol. Earth Syst. Sci., 19, 2079-2100,
850 http://dx.doi.org/10.5194/hess-19-2079-2015.

851 Tardif, R., Hakim, G.J., Snyder, C., (2015). Coupled atmosphere–ocean data assimila-
852 tion experiments with a low-order model and CMIP5 model data, Clim Dyn 45: 1415.
853 https://doi.org/10.1007/s00382-014-2390-3.

854 Terejanu, G.A., (2009). Unscented Kalman filter tutorial, Workshop on Large-Scale Quantifi-
855 cation of Uncertainty, Sandia National Laboratories, pp. 1–6.

856 Thomas, A.C., Reager, J.T., Famiglietti, J.S., Rodell, M., (2014). A GRACE-based water
857 storage deficit approach for hydrological drought characterization. Geophys. Res. Lett. 41,
858 1537–1545.

859 Tian, S., Tregoning, P., Renzullo, L.J., van Dijk, A.I.J.M., Walker, J.P., Pauwels, V.R.N.,
860 Allgeyer, S., (2017). Improved water balance component estimates through joint assimila-
861 tion of GRACE water storage and SMOS soil moisture retrievals, Water Resour. Res., 53,
862 http://dx.doi.org/10.1002/2016WR019641.

Ummenhofer, C.C., England, M.H., McIntosh, P.C., Meyers, G.A., Pook, M.J., Risbey, J.S., Sen Gupta, A., Taschetto, A.S., (2009). What causes southeast Australia's worst droughts? Geophys. Res. Lett. 36, L04706. http://dx.doi.org/10.1029/2008GL036801.

Van der Merwe, R., (2004). Sigma-Point Kalman Filters for probability inference in dynamic state-space models, PhD Thesis, Oregon Health and Science University.

van Dijk, A.I.J.M., (2010). The Australian Water Resources Assessment System: Technical Report 3, Landscape model (version 0.5) Technical Description, CSIRO: Water for a Healthy Country National Research Flagship.

van Dijk, A.I.J.M., Renzullo, L.J., and Rodell, M., (2011). Use of Gravity Recovery and Climate Experiment terrestrial water storage retrievals to evaluate model estimates by the Australian water resources assessment system, Water Resour. Res., 47, W11524, http://dx.doi.org/10.1029/2011WR010714.

van Dijk, A.I.J.M., Peña-Arancibia, J.L., Wood, E.F., Sheffield, J., Beck, H.E., (2013). Global analysis of seasonal streamflow predictability using an ensemble prediction system and observations from 6192 small catchments worldwide, Water Resour. Res., 49, 2729–2746, http://dx.doi.org/10.1002/wrcr.20251.

van Dijk, A.I.J.M., Renzullo, L.J., Wada, Y., Tregoning, P., (2014). A global water cycle reanalysis (2003–2012) merging satellite gravimetry and altimetry observations with a hydrological multi-model ensemble. Hydrol Earth Syst Sci 18:2955–2973. http://dx.doi.org/10.5194/hess-18-2955-2014.

Vrugt, J.A., Diks, C.G., Gupta, H.V., Bouten, W., Verstraten, J.M., (2005). Improved treatment of uncertainty in hydrologic modeling: Combining the strengths of global optimization and data assimilation. Water Resour. Res, 41, W01017, http://dx.doi.org/10.1029/2004WR003059.

Vrugt, J.A., Gupta, H.V., Nuallain, B.O., (2006). Real-time data assimilation for operational ensemble streamflow forecasting, J. Hydrometeorol., 7(3), 548–565, http://dx.doi.org/10.1175/JHM504.1.

Vrugt, J.A., ter Braak, C.J.F., Diks, C.G.H., Schoups, G., (2013). Advancing hydrologic data assimilation using particle Markov chain Monte Carlo simulation: theory, concepts

892 and applications, Advances in Water Resources, Anniversary Issue - 35 Years, 51, 457-478,
893 http://dx.doi.org/10.1016/j.advwatres.2012.04.002.

894 Wahr, J.M., Molenaar, M., Bryan, F., (1998). Time variability of the Earth's gravity field:
895 hydrological and oceanic effects and their possible detection using GRACE. J Geophys Res
896 108(B12):30205–30229, http://dx.doi.org/10.1029/98JB02844.

897 Wan, E., van der Merwe, R., (2000). The unscented Kalman filter for nonlinear estima-
898 tion, Proceedings of the IEEE 2000 Adaptive Systems for Signal Processing, Communica-
899 tions, and Control Symposium (Cat. No.00EX373), Lake Louise, Alta., 2000, pp. 153-158,
900 http://dx.doi.org/10.1109/ASSPCC.2000.882463.

901 Wan, E., van der Merwe, R., (2001). The Unscented Kalman Filter. Wiley Publishing.

902 Weerts, A.H., El Serafy, G.Y.H., (2006). Particle filtering and ensemble Kalman filtering for
903 state updating with hydrological conceptual rainfall-runoff models. Water Resour. Res., 42,
904 W09403, http://10.1029/2005WR004093.

905 Wooldridge, S.A., Kalma, J.D., (2001). Regional-scale hydrological modelling using multiple-
906 parameter landscape zones and a quasi-distributed water balance model. Hydrological Earth
907 System Sciences. 5: 59-74.

908 Yin, J., Zhan, C., Gu, H., et al., (2014). A case study of evapotranspiration data assimilation
909 based bon hydrological model. Advances in Earth Science, 29(9): 1075–1084.

910 Young, P.C., (2002). Advances in real-time flood forecasting. Philos. Trans. Roy. Soc. London,
911 360, 1433–1450.

912 Zaitchik, B.F., Rodell, M., Reichle, R.H., (2008). Assimilation of GRACE terrestrial water stor-
913 age data into a land surface model: results for the Mississippi River Basin. J Hydrometeorol
914 9(3):535–548, http://dx.doi.org/10.1175/2007JHM951.1.

915 Zhang, Y., Bocquet, M., Mallet, V., Seigneur, C., and Baklanov, A., (2012). Real-time air
916 quality forecasting, Part I: History, techniques, and current status, Atmos. Environ., 60,
917 632–655.

918 Zhao, Y., Deng, X., Zhang, S., Liu, Z., Liu, C., Vecchi, G., Han, G., Wu, X., (2017). Impact of

an observational time window on coupled data assimilation: simulation with a simple climate model, Nonlin. Processes Geophys., 24, 681-694, https://doi.org/10.5194/npg-24-681-2017.

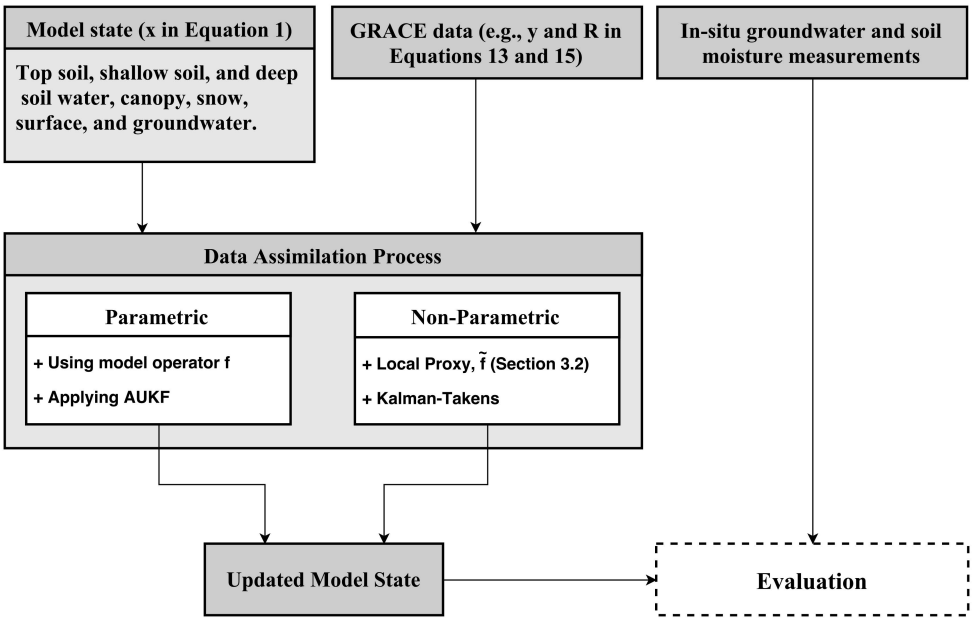

Figure 1: A schematic illustration of the data integration process implemented for this study.

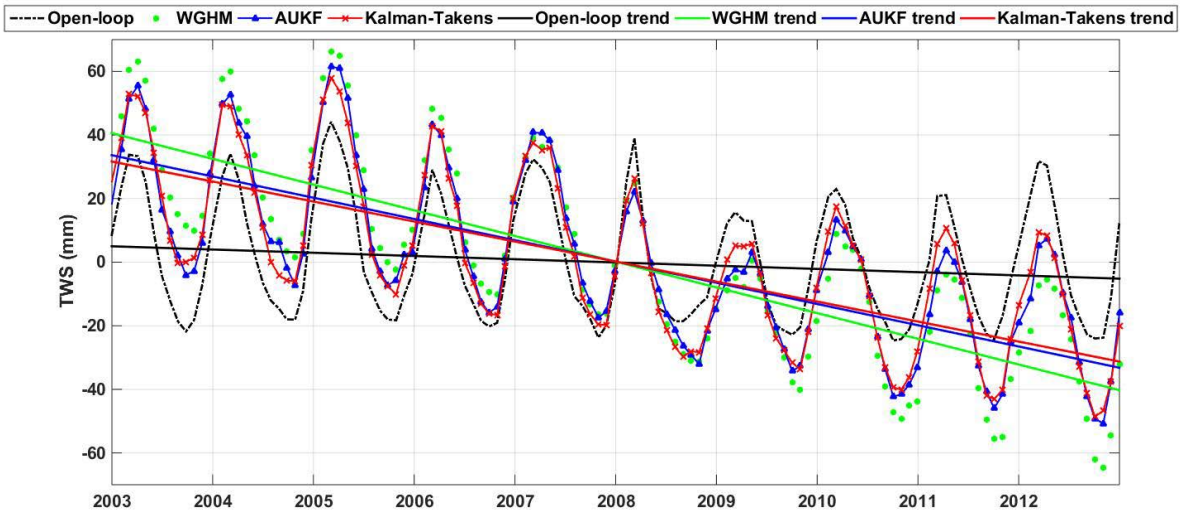

Figure 2: Average TWS variation time series over Iran from AUKF, Kalman-Takens, open-loop run, and WGHM with corresponding trend lines.

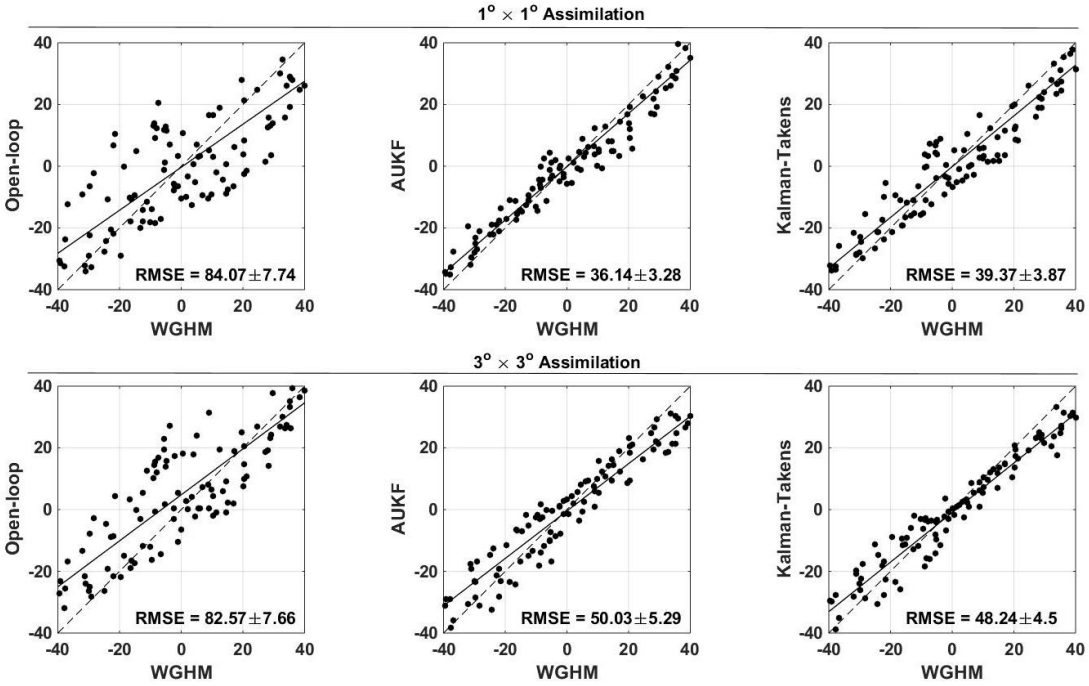

Figure 3: Scatter plots of open-loop, AUKF, and Kalman-Takens TWS estimates with respect to WGHM TWS at the two spatial resolution of 1°×1° and 3°×3°. The presented average RMSE values for each method is calculated based on the original WGHM TWS (before perturbation using GRACE errors). In each sub-figure reference (dashed) and fitted (solid) lines are illustrated.

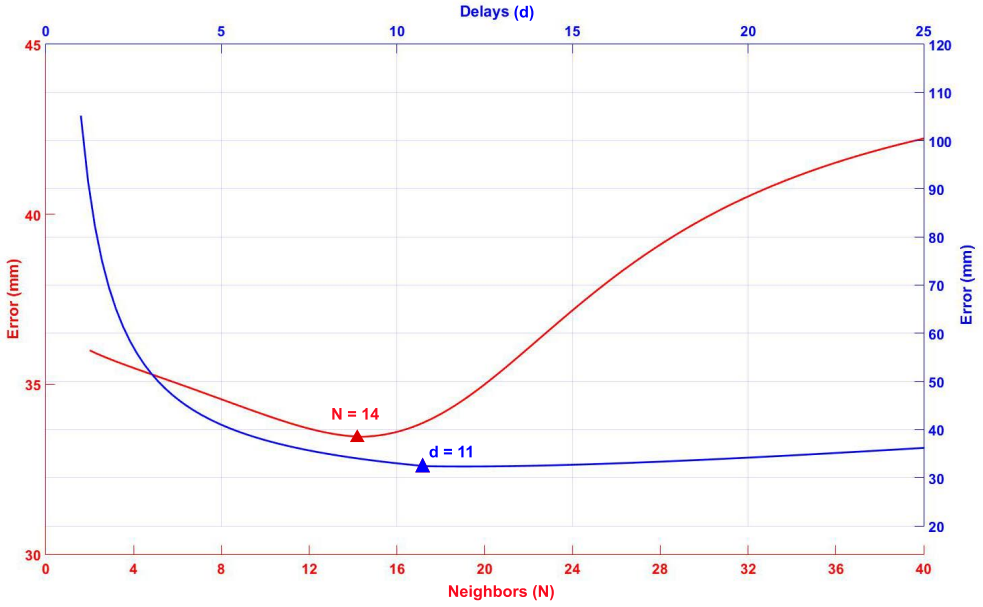

Figure 4: Estimated average errors from different scenarios considered based on the number of neighbors N and delays d. The best estimates are achieved by applying the Kalman-Takens method using $N = 14$ and $d = 11$.

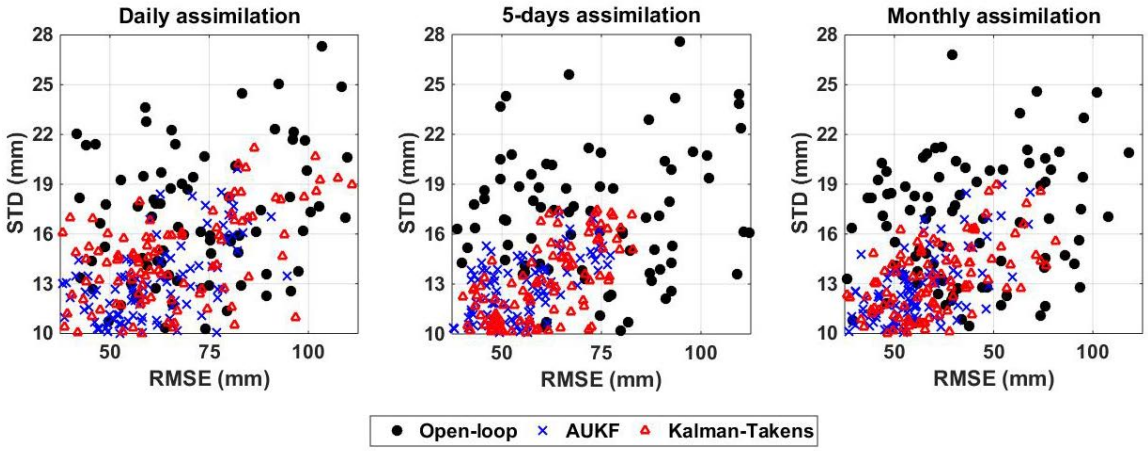

Figure 5: Average groundwater RMSE and STD of from the Kalman-Takens filter, AUKF, and open-loop run computed using groundwater in-situ measurement. The results are presented for assimilation with three different temporal scales (i.e., daily, 5-day, and monthly).

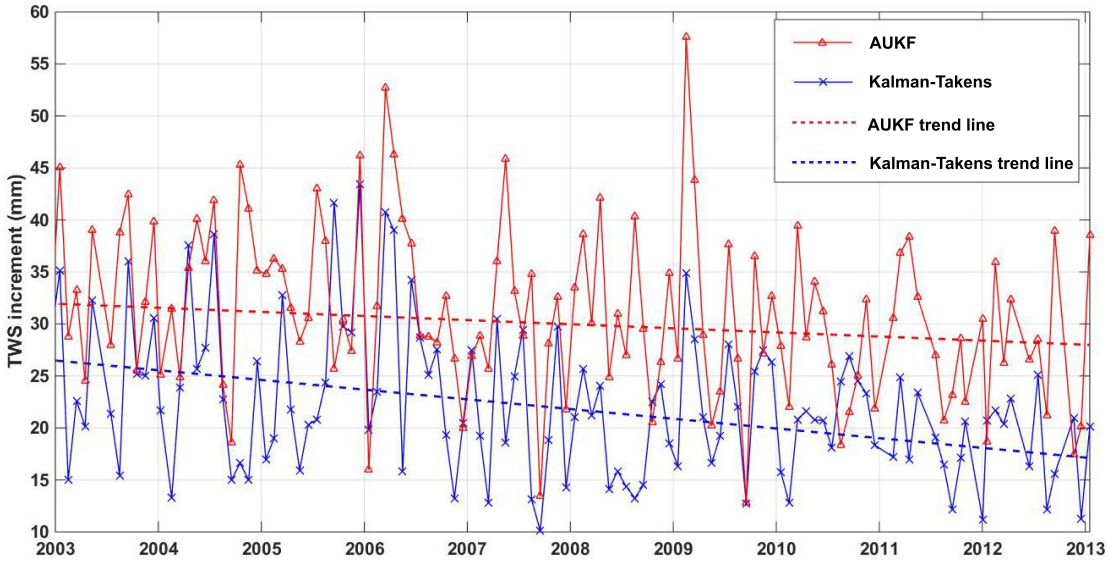

Figure 6: An average TWS increment time series of AUKF and the Kalman-Takens filter on state vectors during the process. Both methods decrease the increment as assimilation proceeds forward in time.

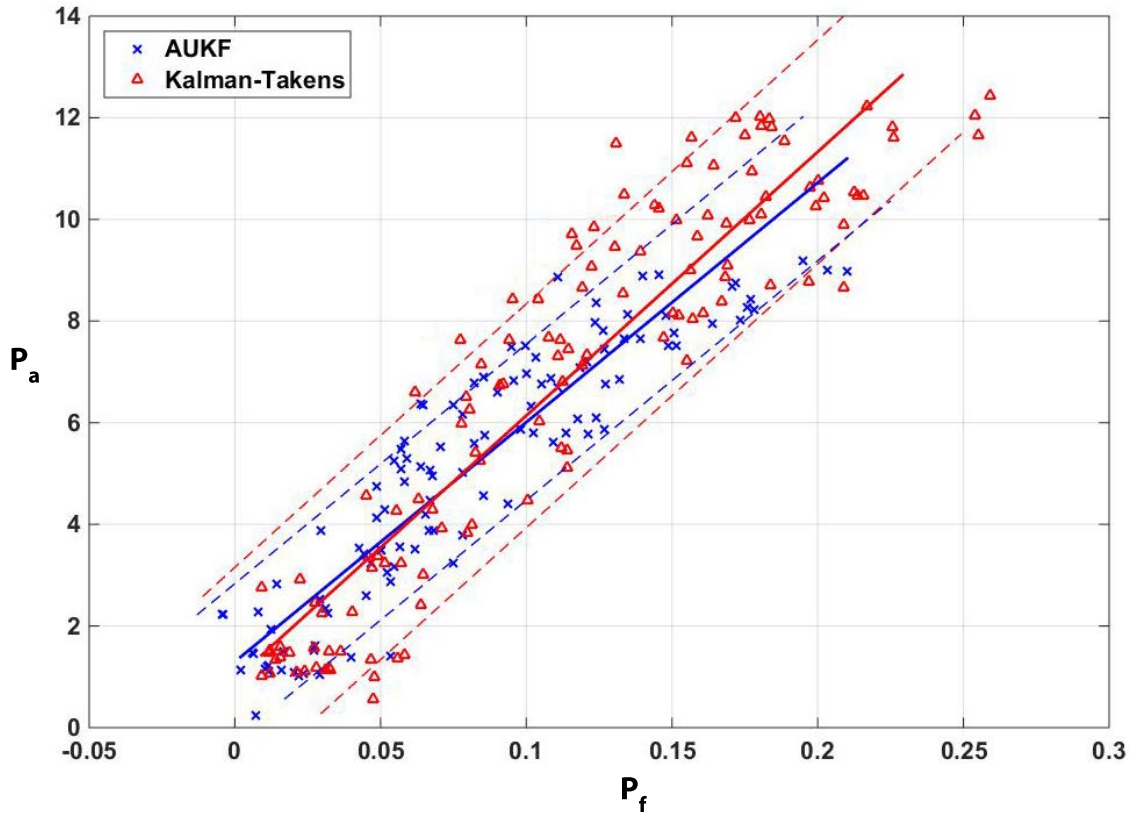

Figure 7: An average estimated covariance matrices of P_f and P_a corresponding to 95% confidence level (dashed lines) at each filtering step using the implemented filters.

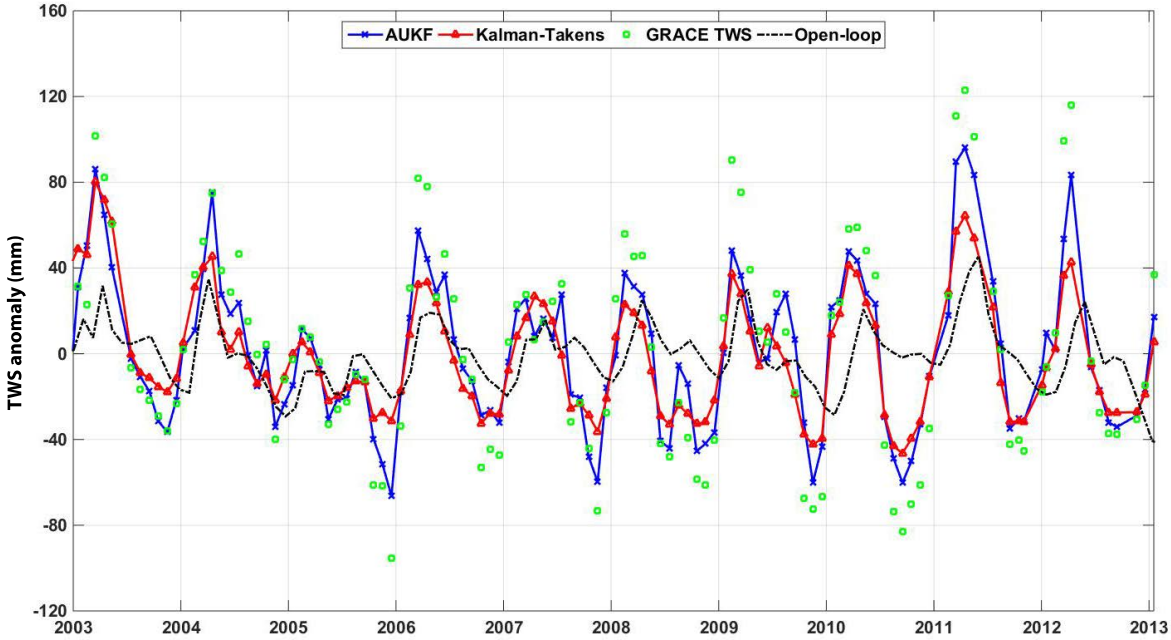

Figure 8: Spatially averaged TWS time series of filters' estimates, GRACE TWS observations, and open-loop run within Australia.

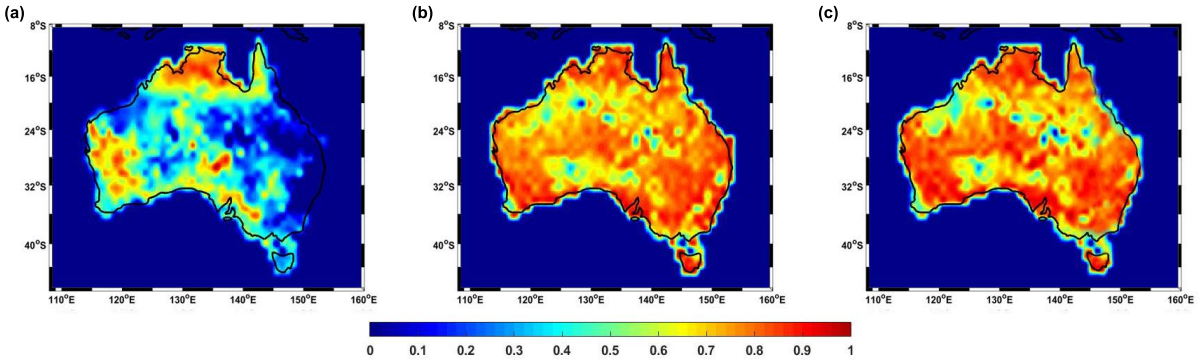

Figure 9: Spatial correlations maps between GRACE TWS and open-loop run (a), AUKF estimates (b), and the Kalman-Takens filter (c).

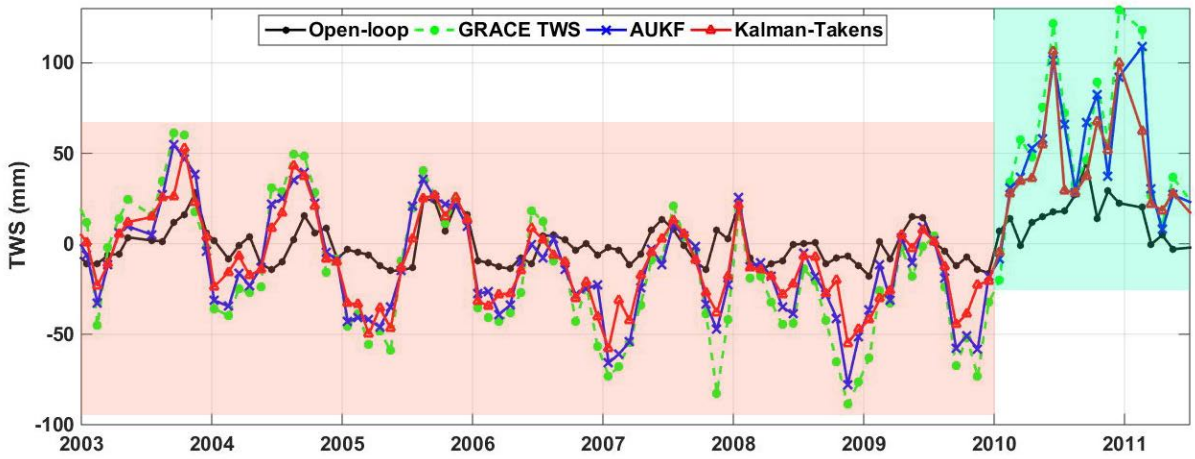

Figure 10: Average TWS variations from the data assimilation filters, open-loop run, and GRACE TWS. The red shaded area shows the Millennium Drought and blue shaded area represent a strong ENSO effect.

Table 1: Summary of statistical values derived from the implemented methods using the groundwater in-situ measurements. The reduction of the RMSE value of the AUKF and Kalman-Takens filters are calculated in relation to the RMSE of the open-loop run.

	Grid-based evaluation			**Basin scale evaluation**		
Metric	**Open-loop**	**AUKF**	**Kalman-Takens**	**Open-loop**	**AUKF**	**Kalman-Takens**
RMSE (mm)	74.57	51.28	53.61	69.40	45.16	46.96
NSE	0.51	0.77	0.75	0.58	0.82	0.81
RMSE reduction (%)	–	31.23	28.11	–	34.93	32.33

Table 2: Summary of NSE values estimated using state estimates derived from implemented methods and the soil moisture in-situ measurements at different layers. The improvements (in %) are calculated based on the increased correlation by applying the methods with respect to the open-loop run.

	Method	**0-8 cm**	**0-30 cm**	**0-90 cm**
	Open-loop	0.59	0.64	0.72
	AUKF	0.63	0.71	0.89
	Kalman-Takens	0.61	0.73	0.85
Improvements (%)	AUKF	6.77	10.94	23.61
	Kalman-Takens	3.39	14.06	18.05